

See discussions, stats, and author profiles for this publication at: <https://www.researchgate.net/publication/263772869>

Experimental and molecular modeling studies of the interaction of the polypyridyl Fe(II) and Fe(III) complexes with DNA and BSA

ARTICLE in SPECTROCHIMICA ACTA PART A MOLECULAR AND BIOMOLECULAR SPECTROSCOPY · JUNE 2014

Impact Factor: 2.35 · DOI: 10.1016/j.saa.2014.06.105

CITATIONS

3

READS

108

9 AUTHORS, INCLUDING:



Jim Simpson

University of Otago

329 PUBLICATIONS 3,225 CITATIONS

[SEE PROFILE](#)



Taghi Khayamian

Isfahan University of Technology

107 PUBLICATIONS 1,562 CITATIONS

[SEE PROFILE](#)



Malihe Ebrahimi

13 PUBLICATIONS 23 CITATIONS

[SEE PROFILE](#)



Hadi Amiri Rudbari

University of Isfahan

161 PUBLICATIONS 518 CITATIONS

[SEE PROFILE](#)



Experimental and molecular modeling studies of the interaction of the polypyridyl Fe(II) and Fe(III) complexes with DNA and BSA



Mohammad Taghi Behnamfar ^a, Hassan Hadadzadeh ^{a,*}, Jim Simpson ^b, Farivash Darabi ^a, Azar Shahpiri ^c, Taghi Khayamian ^a, Malihe Ebrahimi ^a, Hadi Amiri Rudbari ^d, Mona Salimi ^e

^a Department of Chemistry, Isfahan University of Technology, Isfahan 84156-83111, Iran

^b Department of Chemistry, University of Otago, P.O. Box 56, Dunedin 9054, New Zealand

^c Department of Agricultural Biotechnology, College of Agriculture, Isfahan University of Technology, Isfahan 84156-83111, Iran

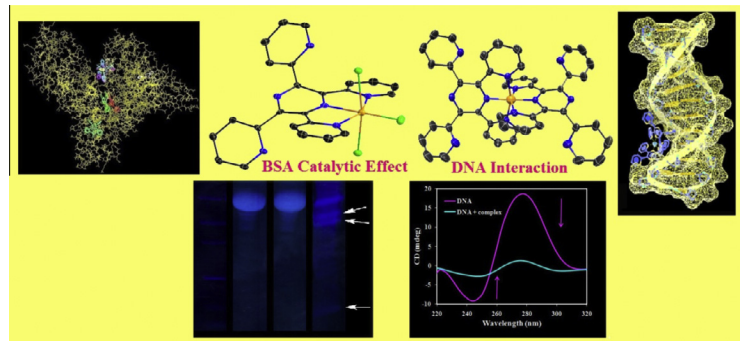
^d Faculty of Chemistry, University of Isfahan, Isfahan 81746-73441, Iran

^e Physiology and Pharmacology Department, Pasteur Institute of Iran, Tehran, P.O. Box 13164, Iran

HIGHLIGHTS

- Two new iron complexes, $[\text{Fe}(\text{tppz})_2](\text{PF}_6)_2 \cdot \text{H}_2\text{O}$ (**1**) and $\text{Fe}(\text{tppz})\text{Cl}_3 \cdot 2\text{CHCl}_3$ (**2**), tppz is (2,3,5,6-tetra(2-pyridyl)pyrazine).
- Binding studies and molecular docking of (**1**) with CT-DNA.
- The results have indicated that (**1**) binds to CT-DNA by three bidding modes.
- The first report about the catalytic effect of polypyridyl metal complexes on the BSA cleavage.
- The molecular docking of (**2**) with BSA.

GRAPHICAL ABSTRACT



ARTICLE INFO

Article history:

Received 28 February 2014

Received in revised form 1 June 2014

Accepted 16 June 2014

Available online 3 July 2014

Keywords:

Iron

2,3,5,6-Tetra(2-pyridyl)pyrazine (tppz)

Catalytic effect

DNA

BSA

Molecular modeling

ABSTRACT

Two mononuclear iron complexes, $[\text{Fe}(\text{tppz})_2](\text{PF}_6)_2 \cdot \text{H}_2\text{O}$ (**1**) and $\text{Fe}(\text{tppz})\text{Cl}_3 \cdot 2\text{CHCl}_3$ (**2**) where tppz is (2,3,5,6-tetra(2-pyridyl)pyrazine), have been synthesized and characterized by elemental analysis, spectroscopic methods (UV-Vis and IR) and single crystal X-ray structure analysis. The interaction of (**1**) as the nitrate salt ($[\text{Fe}(\text{tppz})_2](\text{NO}_3)_2$) with calf-thymus DNA (CT-DNA) has been monitored by UV-Vis spectroscopy, competitive fluorescence titration, circular dichroism (CD), voltammetric techniques, viscosity measurement, and gel electrophoresis. Gel electrophoresis of DNA with $[\text{Fe}(\text{tppz})_2](\text{NO}_3)_2$ demonstrated that the complex also has the ability to cleave supercoiled plasmid DNA. The results have indicated that the complex binds to CT-DNA by three binding modes, viz., electrostatic, groove and partial insertion of the pyridyl rings between the base stacks of double-stranded DNA. Molecular docking of $[\text{Fe}(\text{tppz})_2](\text{NO}_3)_2$ with the DNA sequence d(ACCGACGTCGGT)₂ suggests the complex fits into the major groove. The water-insoluble complex (**2**) can catalyze the cleavage of BSA at 40 °C. There are no reports of the catalytic effect of polypyridyl metal complexes on the BSA cleavage. Molecular docking of (**2**) with BSA suggests that, when the chloro ligands in the axial positions are replaced by water molecules, the BSA can interact with the Fe(III) complex more easily.

© 2014 Elsevier B.V. All rights reserved.

* Corresponding author. Tel.: +98 311 3913240; fax: +98 311 3912350.

E-mail address: hadad@cc.iut.ac.ir (H. Hadadzadeh).

Introduction

Over the course of the past few years, researchers have carried out a wide range of investigations focused on the coordination chemistry and subsequent reactivity of transition metal complexes with nitrogen-containing ligands. Transition metal complexes with nitrogen-containing ligands are potentially useful in a multitude of processes with biological or industrial significance [1–3]. Among these ligands, pyridine-derived polydentate ligands play a fundamental role in inorganic and bioinorganic chemistry and one of the most fascinating molecules of this kind is 2,3,5,6-tetra(2-pyridyl)pyrazine (tppz; Fig. 1). The tppz ligand was first synthesized by Goodwin and co-workers in 1959 [4]. They also reported a series of monodentate complexes of the type $[M(tppz)_2]^{2+}$ (M = first-row transition metals). Little further work on tppz complexes appeared over the next 30 years, but since 1993, many studies on the synthesis and application of the tppz complexes have been reported. Investigation of tppz complexes is very important because of their potential applications in many areas such as the preparation of new materials with desirable photophysical or magnetic properties [5], construction of both methanol-based and proton exchange membrane fuel cells (PEMFCs) [2,6], preparation of carbon-supported catalysts [7], synthesis of supramolecular compounds [8,9], sequestering iron for disease prevention [10], coordination polymers [11], molecular sensors [12], molecular wires [13], photodynamic therapy studies [14], and finally in biochemical studies such as the investigation of DNA- and BSA-binding [15].

DNA-binding studies are very important in the development and advancement of new therapeutic reagents and DNA molecular probes. DNA is the primary intracellular target of anticancer drugs due to its interaction with many small organic compounds and transition metal complexes [16]. The possible interaction model between small molecules and DNA generally follows three patterns: (I) electrostatic binding between the cation species and negatively charged DNA phosphate residues, (II) groove binding in which molecule enters and binds to a groove of the DNA helix through hydrogen bonding and van der Waals interaction forces (duplex DNA forms two distinct grooves, a wider major groove and a narrower minor groove), and (III) intercalative binding between drug and individual base pairs. It has been reported that the intercalating ability of a complex depends on the planarity of ligands, the coordination geometry, ligand donor atom type and the metal ion type [3a,16–22]. *In vitro* DNA binding is an important step to design effective chemotherapeutic agents and anticancer drugs.

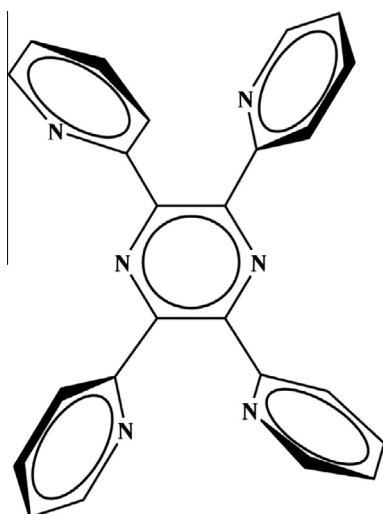


Fig. 1. Molecular structure of tppz.

We are interested in the DNA-binding and cleavage mechanisms of coordination complexes. Therefore mononuclear Fe(II)- and Fe(III)-tppz complexes, were synthesized and characterized by elemental analysis, spectroscopic methods and single-crystal X-ray diffraction. The binding properties of (1) as the nitrate salt with calf-thymus DNA (CT-DNA) under physiological conditions has been studied using UV–Vis spectrophotometry, an ethidium bromide displacement assay (measured by emission quenching), circular dichroism (CD), cyclic voltammetry (CV), differential pulse voltammetry (DPV), DNA solution viscosity measurements and a gel electrophoresis assay. The catalytic effect of (2) on the cleavage of BSA has also been studied. Molecular docking studies were also performed to obtain detailed binding information for the interaction of (1) with DNA and (2) with BSA.

Experimental

Materials and methods

All chemicals and solvents were of high purity and used without any further purification. Highly polymerized calf-thymus DNA (CT-DNA) (Sigma) was used as received. The solutions of CT-DNA gave a UV absorbance ratio (260 over 280 nm) of more than 1.8, indicating its purity [23]. Tris(hydroxymethyl)-aminomethane (Tris) buffer and ethidium bromide (3,8-diamino-5-ethyl-6-phenylphanthridinium bromide, EthBr) were of analytical reagent grade and obtained from Merck. Bovine serum albumin (BSA) and agarose (molecular biology grade) were purchased from Sigma-Aldrich. Doubly-distilled deionized water was used for preparation of all solutions. A stock solution of CT-DNA was prepared by dissolving DNA in 10 mM Tris buffer and 10 mM NaCl at pH 7.2. The DNA concentration per nucleotide was determined by absorption spectroscopy using the molar absorption coefficient ($\varepsilon = 6600 \text{ M}^{-1} \text{ cm}^{-1}$) at 260 nm [24]. The stock solutions were stored at 4 °C and used within 4 days.

Elemental analysis (C, H and N) were performed by using a Leco, CHNS-932 elemental analyzer. Fourier transform infrared spectra were recorded on an FT-IR JASCO 680-PLUS spectrometer in the region of 4000–400 cm^{-1} using KBr pellets. Electronic absorption spectra were recorded on a JASCO 7580 UV–Vis–NIR double-beam spectrophotometer using quartz cells with a path length of 10 mm. Steady state luminescence measurements were performed on a SHIMADZU RF-5000 spectrofluorimeter. Voltammetric experiments were performed on a SAMA Research Analyzer M-500. All measurements were carried out in a 15 mL cell which was fitted with a Teflon lid incorporating a three-electrode system comprising of a platinum electrode ($\phi = 2 \text{ mm}$) as the working electrode, a platinum wire as the auxiliary electrode and a silver wire as the pseudo-reference electrode. The platinum working electrode surface was freshly cleaned with alumina polish on a micro-cloth before each scan and was rinsed with doubly-distilled water between each polishing step. The solutions were deoxygenated by purging with dry N_2 prior to measurements for 30 min and kept under a nitrogen atmosphere throughout all the procedures. Circular dichroism (CD) spectra were measured on a JASCO J-810 spectropolarimeter in a 1 mm path length cylindrical quartz cell. Each sample was scanned from 350 to 190 nm at a speed of 200 nm min^{-1} . The spectral and electrochemical data were collected at the ambient temperature.

Synthesis of $[Fe(tppz)_2](PF_6)_2 \cdot H_2O$ (1)

Complex (1) was prepared by the reaction of tppz (0.388 g, 1 mmol), iron(II) chloride tetrahydrate (0.099 g, 0.5 mmol) and tetrabutylammonium hexafluorophosphate (0.386 g, 1 mmol). The

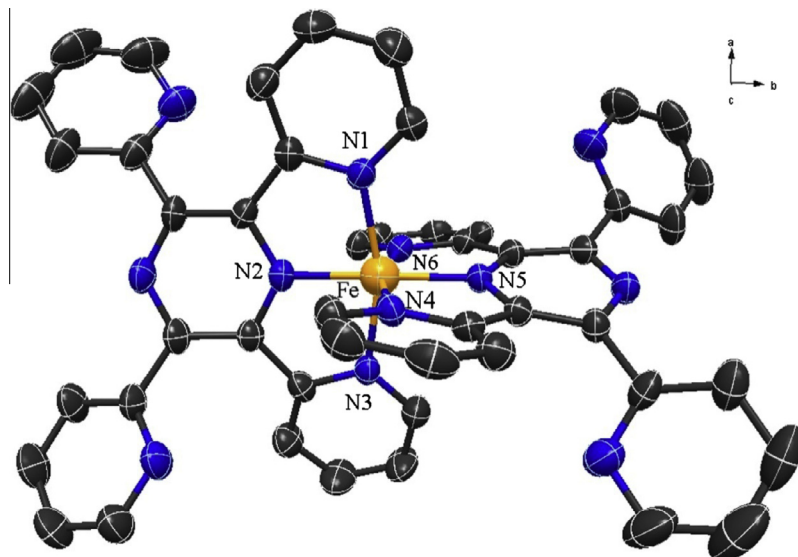
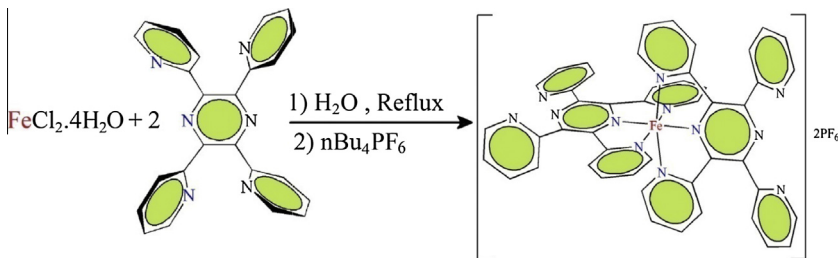


Fig. 2. The molecular structure of (**1**) showing the atom labels and numbering scheme. The hydrogen atoms have been omitted for clarity.



Scheme 1. Synthesis route to (**1**).

tppz ligand and the iron(II) salt were allowed to react in 30 mL of water under refluxing condition until a deep blue solution resulted. Then, tetrabutylammonium hexafluorophosphate dissolved in 15 mL H₂O was added and the color turned to dark purple. The resulting precipitate was filtered and washed with cold water. The precipitate was then dissolved in an acetonitrile/toluene mixture (4:1) and left at room temperature for one week. Dark purple crystals of (**1**) (Fig. 2) suitable for X-ray crystallography were formed. The crystals were washed with cold toluene and air-dried (Scheme 1) (yield 85%; 0.485 g). Anal. Calc. for FeC₄₈H₃₄N₁₂OP₂F₁₂ (MW = 1140.66 g/mol): C, 50.54; H, 3.00; N, 14.73% Found: C, 50.68; H, 2.96; N, 14.64%. FT-IR (KBr pellet, cm⁻¹): 3420 (H₂O), 3071, 1589, 1566, 756, (C=N) and (C=C), 841 (P—F), 670 (Fe—N). UV-Vis (acetonitrile, $\lambda_{\text{max}}/\text{nm}$ ($\varepsilon/\text{M}^{-1} \text{cm}^{-1}$)): 570 (900), 330 (84,800), 286 (85,900), 250 (93,000).

Synthesis of $\text{Fe}(\text{tppz})\text{Cl}_3 \cdot 2\text{CHCl}_3$ (**2**)

Tppz (0.388 g, 1 mmol) was dissolved in 20 mL of ethanol with stirring. To the solution was then added a solution of FeCl₃ (0.162 g, 1 mmol) in 10 mL ethanol. Upon addition, the yellow solution changed to a violet color with the immediate precipitation of a red powder. The reaction mixture was refluxed for 4 h. The resulting precipitate was filtered and washed with ethanol and dried in air at room temperature. The red precipitate was crystallized by slow evaporation of a chloroform solution of the complex at room temperature. After 1 week, red crystals of (**2**) (Fig. 3) suitable for X-ray crystallography were formed (Scheme 2). The complex is stable in the solid state as well as in non-aqueous

solutions. It is not soluble in water (yield: 82%, 0.651 g). Anal. Calc. for FeC₂₆H₁₈N₆Cl₉ (MW = 789.36 g/mol): C, 39.56; H, 2.30; N, 10.65% Found: C, 39.61; H, 2.28; N, 10.69%. FT-IR (KBr pellet, cm⁻¹): 3073, 1598, 1566, 751, (C=N) and (C=C), 666 (Fe—N). UV-Vis (chloroform, $\lambda_{\text{max}}/\text{nm}$ ($\varepsilon/\text{M}^{-1} \text{cm}^{-1}$)): 570 (900), 330 (84,800), 286 (85,900), 250 (93,000).

X-ray structure determination

The dark purple crystals of (**1**) were grown by the slow evaporation of a 4:1 acetonitrile/toluene solution of the complex and the shiny red crystals of (**2**) were grown by the slow evaporation of chloroform solution of the complex. Single crystal X-ray diffraction measurements of the complexes were carried out on two separate Bruker APEX-II CCD diffractometers, using graphite-monochromatized Mo K α radiation ($\lambda = 0.71073 \text{ \AA}$) with data for (**1**) collected at 296(2) K with that for (**2**) collected at 93(2) K. Unit cell parameters were determined by the least-squares calculations with θ angles ranging from 2.2° to 22.5° for (**1**) and 2.4° to 20.4° for (**2**). Absorption corrections were applied based on the semi-empirical multi-scan approach (SADABS) [25]. The structures were solved by direct methods using SHELXS [26] and refined by full-matrix least-squares against F^2 using SHELXL97 with all non-hydrogen atoms refined anisotropically [26]. Hydrogen atoms were located from the difference Fourier syntheses and placed in geometrically calculated positions with isotropic displacement parameters. For **1** a high peak in the difference map following the location of all non-hydrogen atoms of the complex was assigned to the O atom of a solvate water molecule but the H atoms could not be assigned.

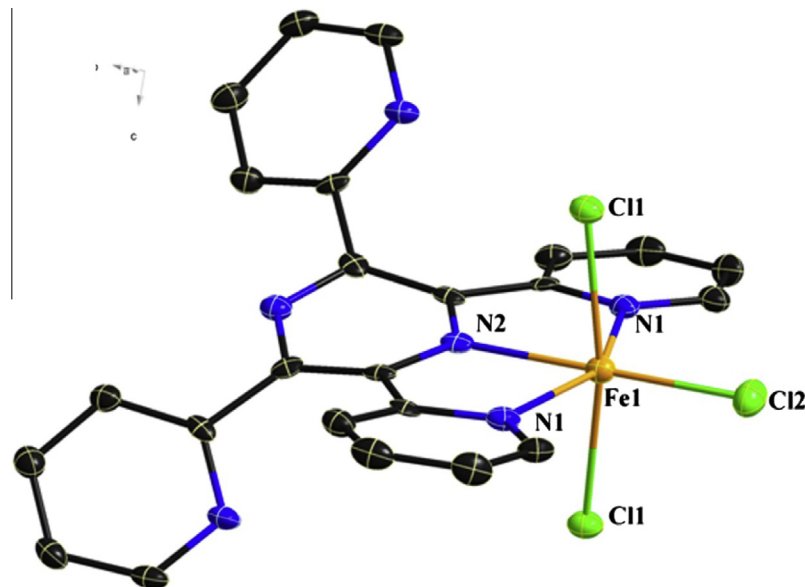
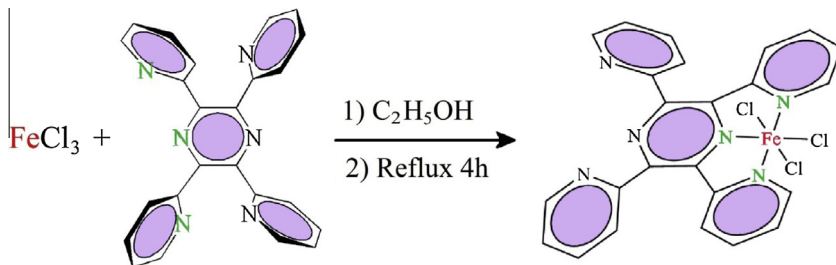


Fig. 3. The molecular structure of (**2**) showing the atom labels and numbering scheme. The hydrogen atoms have been omitted for clarity.



Scheme 2. Synthesis route to (**2**).

For **2**, the Fe^{3+} cation and one of the Cl^- anions lie on a twofold axis with the asymmetric unit comprising only one half of the molecule. Additional high peaks in the difference map of the complex had been found. These were refined to reveal a CHCl_3 solvate molecule so that the molecular formula **2** can be assigned as $\text{C}_{24}\text{H}_{16}\text{Cl}_3\text{FeN}_6\cdot 2(\text{CHCl}_3)$. Final residuals were $R_1 = 0.0529$, $wR_2 = 0.183$ (for 10,329 reflections with $I > 2\sigma(I)$) for (**1**) and $R_1 = 0.028$, $wR_2 = 0.066$ (for 1571 reflections with $I > 2\sigma(I)$) for (**2**). Further details of the structural analyses are given in Table 1. Selected bond lengths, bond angles and torsion angles are listed in Table 2.

DNA binding experiments

All DNA binding experiments, unless otherwise noted were carried out in 10 mM Tris buffer and 10 mM NaCl at pH 7.2. The solubility of (**1**) as the hexafluorophosphate salt was insufficient in the aqueous medium. Thus, for DNA interaction studies, a water-soluble nitrate salt of (**1**), $[\text{Fe}(\text{tpbz})_2](\text{NO}_3)_2$, was used. The hexafluorophosphate salt of complex (**1**) was converted to its nitrate salt by precipitating a solution of the complex in acetone/acetonitrile with $[n\text{-Bu}_4\text{N}]\text{NO}_3$.

The solutions of $[\text{Fe}(\text{tpbz})_2](\text{NO}_3)_2$ were prepared in doubly-distilled deionized water. The spectral features (i.e. UV-Vis spectra) of the complex did not change on keeping its buffered solution for 72 h and no precipitation or turbidity was observed even after long storage at room temperature (at least 2 months after preparation).

This indicates the stability of $[\text{Fe}(\text{tpbz})_2](\text{NO}_3)_2$ in the aqueous media. The absorption titration experiments were conducted by keeping the concentration of $[\text{Fe}(\text{tpbz})_2](\text{NO}_3)_2$ constant (1×10^{-5} M) while varying the DNA concentration from 0 to 2.04×10^{-5} M. For the fluorescence quenching experiments, the DNA solution (5×10^{-5} M) was pretreated with EthBr (5×10^{-6} M) for 1 h. Then the $[\text{Fe}(\text{tpbz})_2](\text{NO}_3)_2$ solution was added to this mixture (from 0.4 to $9.90 \mu\text{M}$) and the variation in the emission intensity was measured after incubation for 2 min. The samples were excited at 520 nm and the emission was observed between 545 and 645 nm. The CD measurements were carried out by keeping the concentration of CT-DNA constant (5×10^{-5} M) with addition of a solution of $[\text{Fe}(\text{tpbz})_2](\text{NO}_3)_2$ and the spectra were recorded in the absence and presence of $[\text{Fe}(\text{tpbz})_2](\text{NO}_3)_2$ with ratio (r_i) of 0 and 1, where $r_i = [\text{complex}] / [\text{DNA}]$. The CV and DPV measurements were recorded by keeping the concentration of $[\text{Fe}(\text{tpbz})_2](\text{NO}_3)_2$ constant (2×10^{-3} M) and adding of a solution of DNA. The supporting electrolyte was a buffer solution containing 10 mM Tris/50 mM NaCl buffer (pH 7.2). The complex-DNA solution was allowed to equilibrate for 10 min at room temperature before each measurement. Viscosity experiments were carried out using a Cannon-Fenske capillary viscometer no. 50 (Schott Geräte). The viscosity of a DNA solution has been measured in the presence of increasing amounts of complex (**1**). The relation between the relative solution viscosity (η / η_0) and DNA length (L / L_0) is given by the equation $L / L_0 = (\eta / \eta_0)^{1/3}$, where

Table 1

Crystal data and structure refinement for (1) and (2).

| Complex | (1) | (2) |
|--|---|---|
| Chemical formula | C ₄₈ H ₃₂ FeN ₁₂ ·2(F ₆ P)·H ₂ O | C ₂₄ H ₁₆ Cl ₃ FeN ₆ ·2(CHCl ₃) |
| Formula weight | 1140.66 | 789.36 |
| Crystal system | Monoclinic | Monoclinic |
| Space group | P2(1)/n | C2/c |
| <i>a</i> (Å) | 11.4914(3) | 8.8909(9) |
| <i>b</i> (Å) | 29.5283(9) | 20.644(2) |
| <i>c</i> (Å) | 14.1580(5) | 17.0980(19) |
| β (°) | 99.979(1) | 93.177(4) |
| <i>V</i> (Å ³) | 4731.4(3) | 3133.4(6) |
| <i>Z</i> | 4 | 4 |
| <i>F</i> ₀₀₀ | 2312 | 1580 |
| <i>D</i> _x (Mg m ⁻³) | 1.601 | 1.673 |
| λ (Mo K α) (Å) | 0.71073 | 0.71073 |
| θ Ranges (°) | 2.2–22.5 | 2.4–20.4 |
| μ (mm ⁻¹) | 0.49 | 1.28 |
| <i>T</i> (K) | 296(2) | 93(2) |
| Crystal size (mm) | 0.58 × 0.32 × 0.18 | 0.40 × 0.13 × 0.06 |
| <i>T</i> _{Min} and <i>T</i> _{Max} | 0.841 and 0.906 | 0.630 and 0.745 |
| Measured reflections | 149,250 | 8131 |
| Independent reflections | 10,329 ($R_{\text{int}} = 0.117$) | 1571 ($R_{\text{int}} = 0.040$) |
| Reflections with <i>I</i> > 2 σ (<i>I</i>) | 5376 | 1384 |
| Index ranges | $-14 \leq h \leq 14$ $-37 \leq k \leq 37$ $-18 \leq l \leq 18$ | $-8 \leq h \geq 8$ $-19 \leq k \geq 20$ $-16 \leq l \geq 16$ |
| <i>R</i> [F^2 > 2 σ (F^2)] | 0.053 | 0.028 |
| <i>wR</i> (F^2) | 0.183 | 0.066 |
| <i>S</i> | 0.90 | 1.06 |
| Parameters | 685 | 192 |
| (Δ/σ) _{max} | <0.001 | 0.001 |
| $\Delta\rho_{\text{max}}$ and $\Delta\rho_{\text{min}}$ (e Å ⁻³) | -0.51/0.53 | -0.27/0.53 |

L_0 denotes the apparent molecular length in the absence of the compound. The obtained data are presented as $(\eta/\eta_0)^{1/3}$ vs. r ($r = [\text{complex}]/[\text{DNA}]$), where η is the viscosity of DNA in the presence of complex (1), and η_0 is the viscosity of DNA alone in the buffer solution.

DNA cleavage studies

pEGFP-N1 DNA (30 ng/μL) in 50 mM Tris-HCl/NaCl buffer (pH = 7.2) was treated with [Fe(tppz)₂](NO₃)₂. The samples were incubated for 3 h, and then the loading buffer was added. The samples were then electrophoresed for 80 min at 135 V on 0.7% agarose gel using Tris-boric acid-EDTA buffer. After electrophoresis, the bands were developed with UV light and photographed. An investigation of the cleavage mechanism of pEGFP-N1 DNA was carried out in the presence of a reaction activator (H₂O₂) and radical scavengers, such as, NaN₃, SOD, and DMSO. Cleavage was initiated by the addition of [Fe(tppz)₂](NO₃)₂ and quenched with 2 μL of the loading buffer.

Catalytic effect on the cleavage of BSA

All BSA solutions were prepared by dissolving BSA in water (0.4 mg/mL) and filtering. The BSA stock solution was stored at 4 °C in the dark and used within 2 h. Three 2.5 mL samples of the BSA stock solution were chosen. The first sample was stored at 4 °C in the dark as control solution I and the second sample was stirred at 40 °C for 3 h in the dark as control solution II. The third sample was used for the investigation of the catalytic effect of (2) on the cleavage of BSA. To this sample, 5×10^{-5} g of (2) was added and the suspension was stirred at 40 °C for 3 h in darkness. Each three protein samples were mixed with loading buffer 1× (60 mM Tris-HCl, 2% SDS, 10% Glycerol and 0.01% bromophenol blue). In order to reduce disulfide bonds, *dithiothreitol* (DTT) was added to the samples. Then the samples were subjected to 12%

SDS-PAGE. Electrophoresis followed after which the gel was stained with Coomassie Blue R250.

Molecular docking

Molecular docking is a method which allows the prediction of the suitable orientations of a ligand to a receptor when they bind to one another to form a stable complex. The molecular docking study was performed by using the Autodock vina software [27]. All molecular images and animations were produced using the Molegro Virtual Docker (MVD) (<http://www.molegro.com/index.php>) and UCSF Chimera [28] packages. The schematic two-dimensional representations of the docking results were performed using LIGPLOT+ [29].

Chemical structures of BSA and DNA

The crystal structures of BSA (PDB ID: 4F5S) and DNA (PDB ID: 423D) with the sequence d(ACCGACGTCGGT)₂ were obtained from the protein data bank at a resolution of 2.47 Å and 1.60 Å, respectively.

Molecular dynamics simulation on BSA and DNA

A molecular dynamics (MD) simulation was carried out on the structures of BSA and DNA in a water box. The MD simulation was performed using the GROMACS 4.5.1 package [30]. The topology parameters of BSA and DNA were created by the GROMOS96 and Amber99 force fields [31], respectively. The interaction parameters were computed using intermolecular (non-bonded) potential represented as a sum of Lennard-Jones (LJ) force and pairwise Coulomb interaction and the long-range electrostatic force determined by the Particle-Mesh Ewald (PME) method [32,33]. The velocity Verlet algorithm was used for the numerical integrations [34], and initial atomic velocities were generated with a Maxwellian distribution at the given absolute temperature [35]. The BSA and DNA systems were restrained to a cubic box with dimensions 8.17 × 8.17 × 8.17 nm³ and 7.54 × 7.54 × 7.54 nm³, respectively. The water molecules were added using a simple charge (SPC216) model [36] and the solvated systems were neutralized by adding sixteen Na⁺ cations to the BSA system and twenty-two Na⁺ cations to the DNA system. Initially, the energy minimization was performed before any positional restraint procedures. Then, the full system was subjected to 6000 ps MD at constant pressure (1 bar) and constant temperature (310 K) using the Berendsen thermostat [37]. The MD simulations and results were carried out on an open SUSE 11.3 Linux with an Intel Core 2 Quad Q6600 2.4 GHz and 4 GB of RAM.

The stability of the two systems and their structural geometries were tested by means of root-mean-square deviations (RMSDs). The RMSDs between the backbone atoms of the trajectory frames of BSA and DNA with the corresponding atoms of the X-ray structure were calculated for each picosecond (ps) of MD simulation. The average RMSD values of the BSA and DNA backbones were calculated to be 8.33 nm and 5.50 nm, respectively. The equilibrated conformations of the BSA and DNA were used for docking.

Results and discussion

Synthesis and crystal structure

The reactions of tppz with FeCl₂·4H₂O and FeCl₃ are shown in **Schemes 1 and 2**, respectively. The tppz complexes were prepared in good yield. The elemental analyses of the complexes were entirely consistent with their proposed compositions and these are confirmed by X-ray crystallography.

Table 2

Selected bond lengths (Å), bond angles (°) and torsion angles (°) for (1) and (2).

| Complex (1) | | | |
|--|------------|--|------------|
| <i>Bond lengths</i> | | | |
| Fe—N1 | 1.963(3) | Fe—N4 | 1.958(3) |
| Fe—N2 | 1.864(3) | Fe—N5 | 1.865(3) |
| Fe—N3 | 1.955(3) | Fe—N6 | 1.964(3) |
| <i>Bond angles</i> | | | |
| N2—Fe—N5 | 178.66(12) | N4—Fe—N6 | 162.31(11) |
| N2—Fe—N4 | 99.33(11) | N3—Fe—N6 | 88.20(11) |
| N5—Fe—N4 | 81.15(11) | N2—Fe—N1 | 81.06(12) |
| N2—Fe—N3 | 81.71(11) | N5—Fe—N1 | 100.20(11) |
| N5—Fe—N3 | 97.02(11) | N4—Fe—N1 | 89.56(11) |
| N4—Fe—N3 | 93.68(11) | N3—Fe—N1 | 162.76(11) |
| N2—Fe—N6 | 98.34(11) | N6—Fe—N1 | 93.83(11) |
| N5—Fe—N6 | 81.16(11) | | |
| <i>Torsion angle</i> | | | |
| N2—C5—C6—N1 | 8.65 | N8—C7—C15—N7 | −146.65 |
| N2—C9—C10—N3 | 10.26 | N8—C8—C20—N9 | −145.29 |
| N5—C29—C30—N4 | 8.17 | N11—C31—C39—N10 | −139.11 |
| N5—C33—C34—N6 | 7.15 | N11—C32—C44—N12 | −135.51 |
| Symmetry codes: (i) $-x + 1, -y + 1, -z + 1$ | | | |
| Complex (2) | | | |
| <i>Bond lengths</i> | | | |
| Fe1—N1 | 2.129(3) | Fe1—Cl1 | 2.3766(9) |
| Fe1—N2 | 2.123(4) | Fe1—Cl2 | 2.2151(14) |
| Fe1—N1 ⁱ | 2.129(3) | Fe1—Cl1 ⁱ | 2.3767(9) |
| <i>Bond angles</i> | | | |
| N2—Fe1—N1 ⁱ | 75.14(8) | N1—Fe1—Cl1 | 87.45(7) |
| N2—Fe1—N1 | 75.13(8) | Cl2—Fe1—Cl1 | 95.19(3) |
| N1 ⁱ —Fe1—N1 | 150.27(16) | N2—Fe1—Cl1 ⁱ | 84.81(3) |
| N2—Fe1—Cl2 | 180.0 | N1 ⁱ —Fe1—Cl1 ⁱ | 87.45(7) |
| N1 ⁱ —Fe1—Cl2 | 104.86(8) | N1—Fe1—Cl1 ⁱ | 89.89(7) |
| N1—Fe1—Cl2 | 104.87(8) | Cl2—Fe1—Cl1 ⁱ | 95.19(3) |
| N2—Fe1—Cl1 | 84.81(3) | Cl1—Fe1—Cl1 ⁱ | 169.62(5) |
| N1 ⁱ —Fe1—Cl1 | 89.89(7) | | |
| <i>Torsion angle</i> | | | |
| N2—C5—C6—N1 | −10.7(4) | N3—C7—C8—N9 | 146.8(3) |
| N2—C5 ⁱ —C6 ⁱ —N1 ⁱ | −10.7(4) | N3—C7 ⁱ —C8 ⁱ —N9 ⁱ | 146.8(3) |
| Symmetry codes: (i) $-x + 2, y, -z + 3/2$ | | | |

Crystal structure of (1) and (2)

A variety of transition metal complexes of the tppz ligand are known with different metal to tppz ratios and modes of binding [38,39]. These fall into three categories with compositions $[M(\text{tppz})]$, $[M(\text{tppz})_2]$, and $[M_2(\mu\text{-tppz})]$ [40], with seven coordination variants among these classes [38]. Complexes of divalent metal cations generally fall into the $[M^{\text{II}}(\text{tppz})_2]^{2+}$ category. The Fe(II) complex reported here (Fig. 2) is a good example of this class of compound, with the Fe(II) center coordinated in a tridentate fashion by one pyrazine and two of the pyridine N atoms of the two tppz ligands in a distorted octahedral geometry. Two hexafluorophosphate anions and a solvent water molecule complete the asymmetric unit of the structure. The Fe—N(pyrazine) bond distances, Table 2, are significantly shorter than the Fe—N(pyridyl) vectors which may result from the stronger π -acceptor characteristics of the pyrazine rings. The 2-fold symmetric Fe(III) complex 2, Fig. 3, binds only one tppz ligand again in a tridentate fashion, with neutrality achieved by coordinating three chloro ligands to form the complex $[\text{Fe}(\text{tppz})\text{Cl}_3]$, which crystallizes with two CHCl_3 solvate molecules. In contrast to 1, the Fe—N(pyrazine) and Fe—N(pyridyl) bond distances in 2 do not differ significantly from one another, Table 2.

Analysis of the conformations of the tppz ligands in the two complexes depend on the relative orientations of the pyrazine and pyridyl rings with fourteen low energy conformations

predicted. These can be further separated into five families [40,41] depending on the orientation of the pyridyl ring N atoms ("up" or "down") with respect to the pyrazine ring plane, with "up" defined as pointing towards the reader.

In order to describe the structural characteristics of the coordinated tppz ligand, the pyrazine and pyridyl rings are marked. The two pyrazine and eight other pyridyl rings are labeled as **A** and **F**, and **B**, **C**, **D**, **E**, **G**, **H**, **I** and **J**, respectively (Fig. 4). The pyridyl rings at the free side of the tppz ligand are roughly planar. However, due to the steric effects between the hydrogen atoms at the 3-pyridyl positions, the tppz ligand as a whole is far from being planar. There are fourteen conformations of tppz and all conformers have the same basic shape, but differ in the relative positions of the four pyridyl nitrogen atoms. The conformers also can be grouped into five families [39–41]. Accordingly, with respect to the torsion angles ($\text{N}2—\text{C}5—\text{C}6—\text{N}1 = 8.65$, $\text{N}2—\text{C}9—\text{C}10—\text{N}3 = 10.26$, $\text{N}8—\text{C}7—\text{C}15—\text{N}7 = −146.65$ and $\text{N}8—\text{C}8—\text{C}20—\text{N}9 = −145.29$) (Table 2), the conformation of tppz in (1) is designated as 3_{XNNX}. The number 3 indicates that the nitrogen atoms in the **B** and **D** rings are "up" and the nitrogen atoms in the **C** and **E** rings are "down" [39]. The letters following the number indicate the direction that the pyridyl nitrogen atom points relative to the center of gravity of the molecule. The letter "X" indicates an "exo" conformation, where the nitrogen is pointed toward the exterior of the molecule (toward the pyrazine nitrogens, i.e., $|\text{N}_{\text{pz}}—\text{C}—\text{C}—\text{N}_{\text{py}}| < 90^\circ$) while the letter "N" shows an "endo" confor-

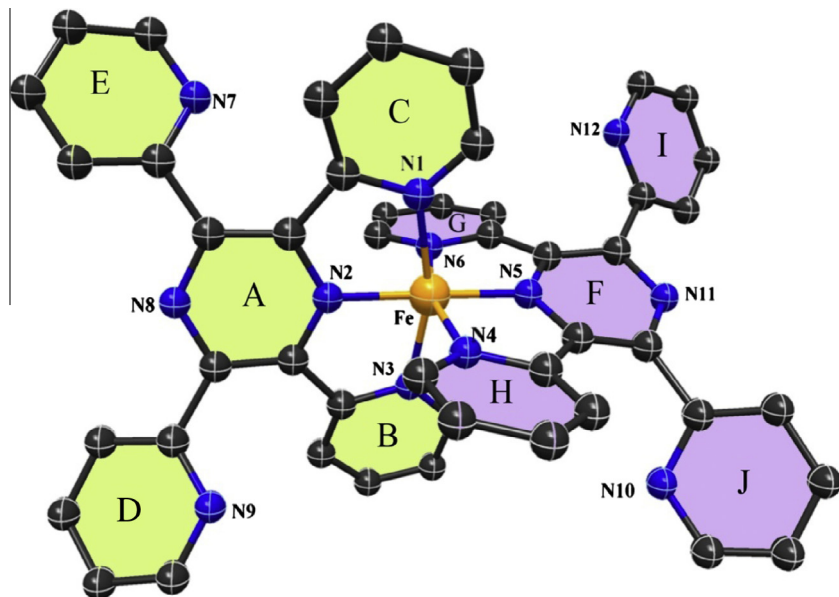


Fig. 4. Representation of the pyridyl rings (**B–E** and **G–J**) and the pyrazine rings (**A** and **F**) in (**1**). The hydrogen atoms have been omitted for clarity.

Table 3

The orientation of the pyridyl rings (**B–E** and **H–J**) with respect to the pyrazine rings (**A** and **F**) in (**1**) (see Fig. 4) and orientation of the pyridyl rings (**B–E**) with respect to the pyrazine ring (**A**) in (**2**) (see Fig. 5).

| Rings | Angle (°) | Rings | Angle (°) |
|--------------------|-----------|------------|-----------|
| <i>Complex (1)</i> | | | |
| A F | 68.14 | A D | 36.02 |
| B C | 4.76 | A E | 35.69 |
| G H | 12.10 | F G | 20.53 |
| D E | 27.58 | F H | 23.83 |
| I J | 43.34 | F I | 41.23 |
| A B | 16.91 | F J | 44.75 |
| A C | 19.93 | | |
| <i>Complex (2)</i> | | | |
| BC | 2.81 | AC | 18.22 |
| DE | 25.21 | AD | 34.52 |
| AB | 18.22 | AE | 34.52 |

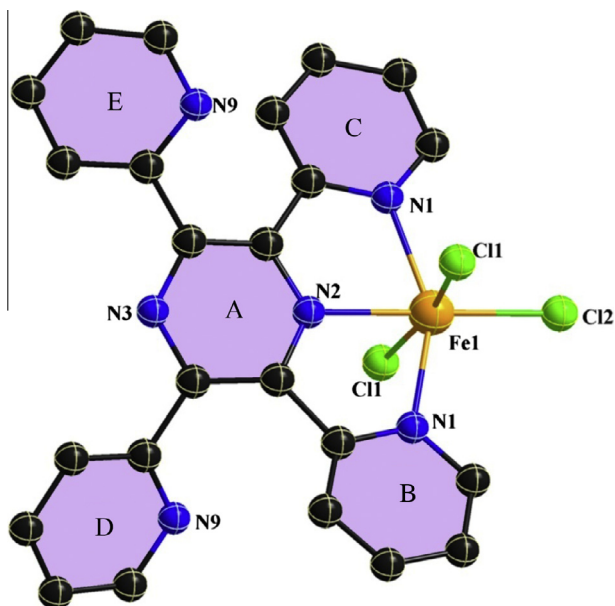


Fig. 5. Representation of the pyridyl rings (**B–E**) and the pyrazine rings (**A**) in (**2**). The hydrogen atoms have been omitted for clarity.

tion, where it is pointed toward the interior of the molecule ($|N_{pz}—C—C—N_{py}| > 90^\circ$). Conformer 3_{XNNX} is one of the most stable conformations for the tppz ligand [39–41]. It deserves to be noted that the free N7 and N9 pyridyl nitrogen atoms are “up” and “down” from the pyrazine ring. The dihedral angles between the mean planes of the pyridyl rings are listed in Table 3. The uncoordinated pyridyl nitrogen atoms (N7, N9, N10 and N12) are slightly shifted “up” and “down” from the respective pyrazine ring. But the other nitrogen atoms (N1, N3, N4 and N6,) are placed on the same side of the respective pyrazine rings.

For compound **2**, the plane encompassing the pyrazine ring **A** and coordinated pyridyl rings **B** and **C**, Fig. 5, shows a maximum deviation of $0.364(3)\text{ \AA}$ for atom C7 of the pyrazine ring which itself deviates considerably from planarity (rms deviation 0.086 \AA). The dihedral angle between the planes of the **A** and **B** pyridyl rings is $2.8(1)^\circ$ further emphasizing the relative planarity of this coordination plane. The N2—C5—C6—N1 and N3—C7—C8—N9 torsion angles are $10.7(4)^\circ$ and $146.8(3)^\circ$ respectively such that, using the notation suggested by Padgett et al. [39], the tppz conformation in molecule (**2**) is designated as 3_{XNNX} .

UV–Vis and IR spectroscopic studies

The electronic absorption spectrum of (**1**) was recorded in acetonitrile and shows a weak broad absorption band in the visible region (575 nm) which can be assigned to a $d-d$ transition. The intense absorption bands seen in the UV region most likely arise from the spin-allowed, ligand-centered (LC) ($\pi \rightarrow \pi^*$ and $n \rightarrow \pi^*$) transitions. The electronic spectrum of (**2**) was determined in chloroform solution. The spectrum shows a weak broad band in 520–600 nm and an intense triple band at 230–340 nm. The former can also be attributed to the $d-d$ transition, and the latter to ligand-centered ($\pi \rightarrow \pi^*$) and ($n \rightarrow \pi^*$) transitions [42].

For the free tppz ligand, the predominant vibrations are associated with $\nu(C=C)$, $\nu(C=N)$, and ring stretching modes. The reported separation between $\nu(C=C)$ and $\nu(C=N)$ vibrations is close to 20 cm^{-1} for polypyridyl ligands [43,44], and thus, for complex (**1**), the observed vibrational absorption bands for tppz at 1589 and 1566 cm^{-1} may be due to either different $\nu(C=N)$ modes of the pyrazine and pyridyl rings or $\nu(C=C)$ and $\nu(C=N)$ modes with coincidental equivalence of the different rings [44]. An intense

band at 1391 cm^{-1} is assigned to ring stretching of both the pyrazine and pyridyl rings of tppz. The FT-IR spectrum of (**1**) (Fig. S1, see Supplementary Materials) shows an absorption pattern in the $4000\text{--}400\text{ cm}^{-1}$ region similar to that of the tppz ligand. The strong absorption band at 841 cm^{-1} is assigned to $\nu(\text{P}-\text{F})$ of the PF_6^- counteranions and the medium absorption band at 670 cm^{-1} is assigned to $\nu(\text{Fe}-\text{N})$ [44]. The IR spectrum of (**2**) (Fig. S2, see Supplementary Materials) showed vibration bands appearing for tppz at 1598 and 1566 cm^{-1} may be due to either different $\nu(\text{C}=\text{N})$ vibrations of the pyrazine and pyridyl rings or $\nu(\text{C}=\text{C})$ and $\nu(\text{C}=\text{N})$ vibrations with coincidental equivalence of the different polypyridyl rings [44]. The free tppz also displays an intense band at 1402 cm^{-1} , assignable to the ring stretching frequency of both pyrazine and pyridyl rings. The absorption bands at 666 and 427 cm^{-1} is assigned to $\nu(\text{Fe}-\text{N})$ and $\nu(\text{Fe}-\text{Cl})$ respectively [44].

DNA-binding studies

Study of the interactions of DNA with transition metal complexes is very important in investigation species that could be used in the treatment all types of cancer [16c]. Many analytical techniques have been used to investigate such interactions such as UV-Vis, fluorescence, circular dichroism (CD) spectropolarimetry, cyclic and differential voltammetry and gel electrophoresis assays. In this study, the following experiments have been used to characterize and distinguish the binding mode of the nitrate salt of (**1**), $[\text{Fe}(\text{tppz})_2](\text{NO}_3)_2$, to CT-DNA.

Absorption spectroscopic studies

A UV-Vis absorption titration can be used to investigate the interaction of metal complexes with DNA. The absorption spectra of $[\text{Fe}(\text{tppz})_2](\text{NO}_3)_2$ in the absence and presence of DNA (at constant concentration of the complex) are shown in Fig. 6. The absorption spectrum of the pure complex displays an intense intraligand $\pi \rightarrow \pi^*$ transition at $\lambda = 203\text{ nm}$, two intraligand $n \rightarrow \pi^*$ transitions around 338 nm , and a $d-d$ transition in 575 nm . In the presence of increasing concentrations of CT-DNA, a hyperchromic shift in the $d-d$ transitions ($\lambda = 575\text{ nm}$) together with a slight red-shift (1 nm) is observed (Fig. 6). When the complex is bound to DNA via an electrostatic binding mode (external contact), hyperchromism in the absorption spectra can occur [45,46]. This hyperchromic effect may be due to the electrostatic interaction between the positively charged $[\text{Fe}(\text{tppz})_2]^{2+}$ unit and the negatively charged phosphate backbone of the DNA helix.

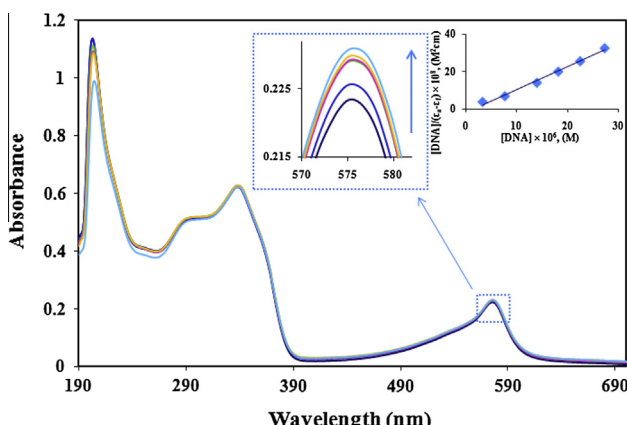


Fig. 6. Electronic absorption spectra for titration of $[\text{Fe}(\text{tppz})_2](\text{NO}_3)_2$ ($1 \times 10^{-5}\text{ M}$) with increasing amounts of CT-DNA ($[\text{DNA}] = 0.0, 1.1, 7.71, 9.9, 12.1$, and $20.4\text{ }\mu\text{M}$, respectively). The arrows show the intensity changes with increasing CT-DNA concentration. Inset: plot of $[\text{DNA}] / (\varepsilon_a - \varepsilon_f)$ vs. $[\text{DNA}]$.

However, the band at 203 nm is decreased in the presence of increasing concentrations of CT-DNA. This hypochromism accompanied by a slight red-shift (2 nm) can be attributed to the partial insertion of the tppz aromatic rings to the ds-DNA [45,47,16]. As can be seen from the crystal structure of the complex (Fig. 2) and the angles between the ring planes (Table 3), the tppz ligands are certainly not planar. Therefore, intercalation for this complex is difficult. It should be also mentioned here that the geometry, size and hydrophobicity of the tppz ligand facilitate binding of the complex into a DNA groove [48].

In order to further investigate the intensity of the interaction between $[\text{Fe}(\text{tppz})_2](\text{NO}_3)_2$ and CT-DNA, the intrinsic binding constant, K_b , was calculated using Eq. (1) [49] (Fig. 6).

$$[\text{DNA}] / (\varepsilon_a - \varepsilon_f) = [\text{DNA}] / (\varepsilon_b - \varepsilon_f) + 1 / K_b (\varepsilon_b - \varepsilon_f) \quad (1)$$

where ε_a , ε_b , and ε_f are the apparent, bound and free Fe(II) complex extinction coefficients, respectively. In particular, ε_f was determined by a calibration curve of the isolated Fe(II) complex in an aqueous solution, following Beer's law. The apparent extinction coefficient, ε_a , was determined as the ratio between the observed absorbance (A_{obs}) and the complex concentration, $A_{\text{obs}} / [\text{Fe(II)} \text{ complex}]$. A plot of $[\text{DNA}] / (\varepsilon_a - \varepsilon_f)$ vs. $[\text{DNA}]$ gives a slope of $1 / (\varepsilon_b - \varepsilon_f)$ and a y-intercept equal to $1 / K_b (\varepsilon_b - \varepsilon_f)$; K_b is the ratio of the slope to y-intercept (Fig. 6). The K_b value for the complex is found to be $2.9 \times 10^5\text{ M}^{-1}$. This value indicates a high affinity of the complex for binding to DNA.

Fluorescence spectroscopic studies

In order to provide further evidence for the interaction mode, binding of $[\text{Fe}(\text{tppz})_2](\text{NO}_3)_2$ to CT-DNA has been studied by a competitive binding fluorescence experiment using ethidium bromide (EthBr) as a probe ($[\text{DNA}] / [\text{EthBr}] = 10$). EthBr, one of the most sensitive fluorescent probes, does not have any appreciable emission in an aqueous solution. However, EthBr produces an intense fluorescence in the presence of DNA due to the intercalation of the phenanthridine ring between the adjacent DNA base pairs. This fluorescence emission can be quenched by the addition of a metal complex due to the replacement of EthBr, and/or electron transfer [50]. Consequently, the degree of quenching can be used to determine the extent of binding between the metal complex and DNA. When the complex is added to CT-DNA pretreated with the EthBr solution ($[\text{DNA}] / [\text{EthBr}] = 10$), the emission intensity of the DNA-EthBr system decreased gradually (Fig. 7). This change in the fluorescence intensity indicates that $[\text{Fe}(\text{tppz})_2](\text{NO}_3)_2$ can replace EthBr from the DNA-EthBr system. The classical Stern-Volmer equation can be used to qualitatively assess the extent of the quenching (Eq. (2)).

$$F_0 / F = 1 + K_q \tau_0 [Q] = 1 + K_{sv} [Q] \quad (2)$$

where $[Q]$ is the concentration of Fe(II) complex (quencher), and F_0 and F are the fluorescence intensities in the absence and presence of the Fe(II) complex, respectively. K_q is the bimolecular quenching constant and τ_0 is the lifetime of the fluorophore in the absence of quencher (Fe(II) complex). Since a fluorescence lifetime is typically near 10^{-8} s , the bimolecular quenching constant (K_q) is calculated from $K_{sv} = K_q \tau_0$ [51]. The fluorescence quenching curve of the DNA-bound EthBr by the complex (Fig. 7) illustrates a good agreement ($R^2 = 0.99$) with the linear curve of the Stern-Volmer equation and $K_{sv} = 6.25 \times 10^4\text{ M}^{-1}$ is calculated by the ratio of the slope to intercept. The large value of K_{sv} indicates that the complex is bound to CT-DNA. Since EthBr was not completely displaced by the complex, a partial intercalation of the complex with DNA is suggested [52]. According to Eq. (2), K_q was determined as $6.25 \times 10^{12}\text{ M}^{-1}\text{ s}^{-1}$, which is greater than the limiting diffusion rate constant ($2.0 \times 10^{10}\text{ M}^{-1}\text{ s}^{-1}$) for a biomacromolecule, indicating the existence of a static quenching mechanism [53]. Fluorescence quench-

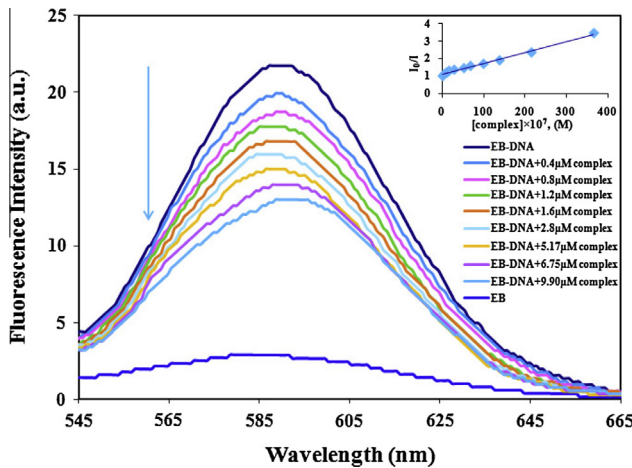


Fig. 7. Emission spectra of the EthBr–DNA system in the absence and presence of various concentrations of $[\text{Fe}(\text{tppz})_2](\text{NO}_3)_2$ in 10 mM Tris–HCl/10 mM NaCl buffer solution. $[\text{DNA}] = 5 \times 10^{-5}$ M, $[\text{EthBr}] = 5 \times 10^{-6}$ M, and $\lambda_{\text{ex}} = 520$ nm. The arrow shows the intensity changes on increasing the complex concentration. Inset: Plot of F_0/F vs. $[\text{complex}]$.

ing can classify into two major mechanisms, viz. a dynamic quenching and a static quenching. In a dynamic quenching mechanism, the fluorophore and the quencher collide to each other in the excited state and in a static quenching mechanism, the fluorophore and the quencher form a complex in the ground state [54].

The binding constant of the complex with DNA in the presence of EthBr may be obtained as follows [55,56]. The reaction of drug molecules (D) with the DNA modified by EthBr (N) can be expressed as:



The binding constant (K_A^n) for this reaction is:

$$K_A^n = \frac{[ND_n]}{[D_f]^n [N_f]} \quad (4)$$

$[D_f]$ is the concentration of the free drug (Fe(II) complex) and $[N_f]$ is the concentration of the DNA–EB complex.

Based on Eq. (4), the following relationship is found [55,56]:

$$\log \frac{F_0 - F}{F} = n \log K_A + n \log \left([D_f] - n[N_f] \frac{F_0 - F}{F_0} \right) \quad (5)$$

where $[N_f]$ and $[D_f]$ are the total concentration of the DNA–EB complex and the free drug (Fe(II) complex), respectively. On the assumption that n in the bracket is equal to 1, the curve $\log (F_0 - F)/F$ vs. $\log([D_f] - n[N_f](F_0 - F)/F_0)$ is drawn and fitted linearly, the slope n can then be obtained. If the slope n obtained is not equal to 1, then it is substituted into the bracket and the curve $\log (F_0 - F)/F$ vs. $\log([D_f] - n[N_f](F_0 - F)/F_0)$ is drawn again. Such the above process is repeated iteratively until an unchanging value of n is determined. Based on the intercept and n , K_A can be obtained. The plots of $\log (F_0 - F)/F$ vs. $\log([D_f] - n[N_f](F_0 - F)/F_0)$ for the DNA–drug complex in the presence of EthBr are shown in Fig. 8, and the binding constant, K_A and n are obtained $1.18 \times 10^5 \text{ M}^{-1}$ and 1.8, respectively.

Circular dichroism spectral studies

The circular dichroism (CD) of double-stranded CT-DNA exhibits a positive CD band at 275 nm for the nucleobase stacking and a negative band at 246 nm for the helix B conformation [57]. Variation in the CD spectrum of DNA during the complex–DNA interaction can be used to distinguish the binding modes of $[\text{Fe}(\text{tppz})_2](\text{NO}_3)_2$ with DNA. Upon the addition of the complex to

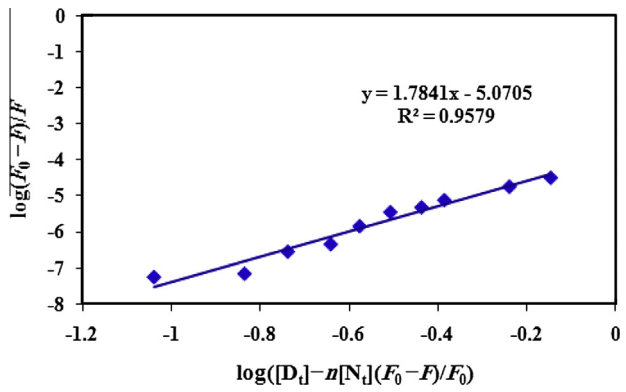


Fig. 8. A plot of $\log ((F_0 - F)/F)$ vs. $([D_t] - n[N_t](F_0 - F)/F_0)$ for $[\text{Fe}(\text{tppz})_2](\text{NO}_3)_2$.

a solution of CT-DNA, the intensities of both positive and negative CD bands are significantly decreased and approach to zero (Fig. 9, and Fig. S3 in Supplementary Materials). This DNA conformational variation clearly indicates the intercalation interaction between the Fe(II) complex and DNA [58–60].

Electrochemical studies

Cyclic and differential pulse voltammetric (CV and DPV) techniques have been employed to study the interaction of redox active complexes with DNA in order to confirm the DNA binding modes suggested by the spectroscopic studies [60].

The cyclic voltammograms of $[\text{Fe}(\text{tppz})_2](\text{NO}_3)_2$ (2.0×10^{-3} M) in the absence and presence of CT-DNA in 10 mM Tris/50 mM NaCl buffer (pH = 7.2) were recorded in the range of +0.18 to −0.16 V with a scan rate of 0.1 V s^{-1} (Fig. 10A). The cyclic voltammogram of the complex in the absence of DNA exhibits a quasi-reversible one-electron wave for the $\text{Fe}^{III}/\text{Fe}^{II}$ couple [61]. The cathodic and anodic peak potentials appear at $E_{pc} = -0.062 \text{ V}$ and $E_{pa} = 0.109 \text{ V}$ with $i_{pc} = 78.766 \mu\text{A}$ and $i_{pa} = -156.25 \mu\text{A}$, respectively. Addition of $33 \mu\text{M}$ DNA to the complex solution causes a decrease in both the cathodic and anodic current ($i_{pc} = 73.181 \mu\text{A}$ and $i_{pa} = -$

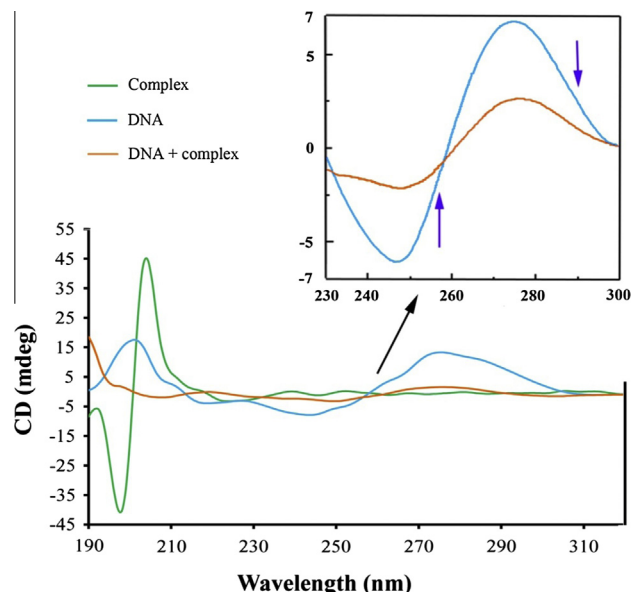


Fig. 9. Circular dichroism (CD) spectra of $[\text{Fe}(\text{tppz})_2](\text{NO}_3)_2$ (green), CT-DNA (5×10^{-5} M) (blue), and DNA + Fe(II) complex (brown). ($r_i = [\text{Fe(II) complex}] / [\text{DNA}] = 0$, and 1). (For interpretation of the references to color in this figure legend, the reader is referred to the web version of this article.)

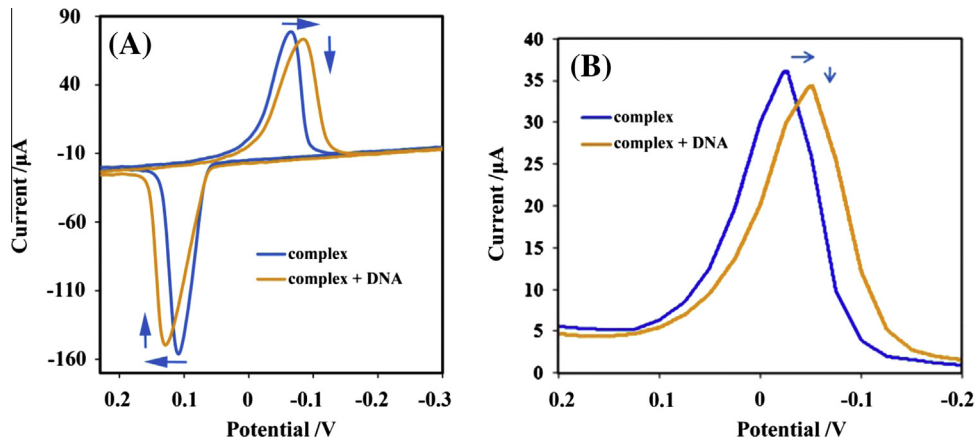


Fig. 10. (A) Cyclic voltammograms of $[\text{Fe}(\text{tppz})_2](\text{NO}_3)_2$ (2.0×10^{-3} M) in the absence and presence of $33 \mu\text{M}$ CT-DNA in 10 mM Tris buffer/ 50 mM NaCl (scan rate = 0.1 V/s). (B) DPVs of $[\text{Fe}(\text{tppz})_2](\text{NO}_3)_2$ (2.0×10^{-3} M) in the absence and presence of $33 \mu\text{M}$ CT-DNA in 10 mM Tris buffer/ 50 mM NaCl (scan rate = 0.05 V/s).

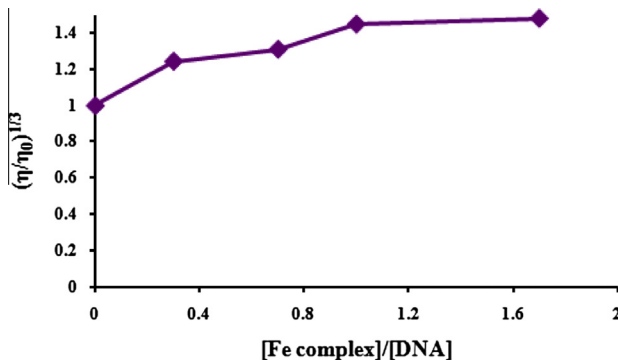


Fig. 11. Relative viscosity of CT-DNA $(\eta/\eta_0)^{1/3}$ in 10 mM Tris-HCl/ 10 mM NaCl buffer solution in the presence of $[\text{Fe}(\text{tppz})_2](\text{NO}_3)_2$ at increasing amounts r ($r = [\text{complex}]/[\text{DNA}]$).

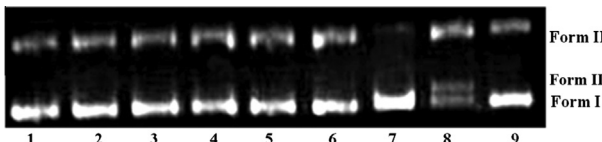


Fig. 12. Gel electrophoresis diagrams showing the cleavage of pEGFP-N1 DNA ($30 \text{ ng}/\mu\text{L}$) at different concentrations of $[\text{Fe}(\text{tppz})_2](\text{NO}_3)_2$ in Tris-HCl/NaCl buffer ($\text{pH} = 7.2$) at 37°C for 3 h and in the absence and presence of standard radical scavengers. Lane 1: DNA control; Lane 2: DNA + complex ($5 \mu\text{M}$); Lane 3: DNA + complex ($10 \mu\text{M}$); Lane 4: DNA + complex ($30 \mu\text{M}$); Lane 5: DNA + complex ($60 \mu\text{M}$); Lane 6: DNA + complex ($100 \mu\text{M}$); Lane 7: DNA + Na_3 ($400 \mu\text{M}$) + complex ($100 \mu\text{M}$); Lane 8: DNA + SOD(15 U) + complex ($100 \mu\text{M}$); Lane 9: DNA + DMSO ($400 \mu\text{M}$) + complex ($100 \mu\text{M}$), respectively.

$-149.38 \mu\text{A}$). Furthermore, the peak potential, E_{pc} , shifts to a more negative potential ($E_{pc} = -0.086 \text{ V}$), while the anodic peak potential, E_{pa} , shifts to a more positive potential ($E_{pa} = 0.130 \text{ V}$). The observed decrease in the both cathodic and anodic currents is related to the interaction between the complex and DNA and this can be explained by slow diffusion of the complex-DNA system to the electrode surface [60]. As proposed by Bard et al. [62], an electrostatic binding mode between molecules and DNA causes a more negative shift in the formal potential (E^0), while an intercalative binding mode results in an E^0 shift to a more positive potential. In the presence of DNA, the CV behavior of the complex exhibits a negative shift of E_{pc} and a positive shift of E_{pa} . Therefore, this result could imply that the molecule can bind to DNA by both intercalation and electrostatic interactions [45,63].

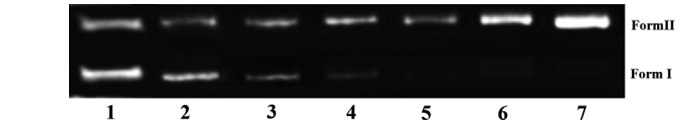


Fig. 13. Agarose gel electrophoresis pattern for the cleavage of pEGFP-N1 DNA ($30 \text{ ng}/\mu\text{L}$) by $[\text{Fe}(\text{tppz})_2](\text{NO}_3)_2$ at different concentrations in Tris-HCl/NaCl buffer ($\text{pH} = 7.2$) at 37°C for 3 h in the presence of H_2O_2 . Lane 1: DNA control; Lane 2: DNA + H_2O_2 ($400 \mu\text{M}$); Lane 3: DNA + H_2O_2 ($400 \mu\text{M}$) + complex ($0.1 \mu\text{M}$); Lane 4: DNA + H_2O_2 ($400 \mu\text{M}$) + complex ($0.5 \mu\text{M}$); Lane 5: DNA + H_2O_2 ($400 \mu\text{M}$) + complex ($1 \mu\text{M}$); Lane 6: DNA + H_2O_2 ($400 \mu\text{M}$) + complex ($2 \mu\text{M}$); Lane 7: DNA + H_2O_2 ($400 \mu\text{M}$) + complex ($3 \mu\text{M}$), respectively.

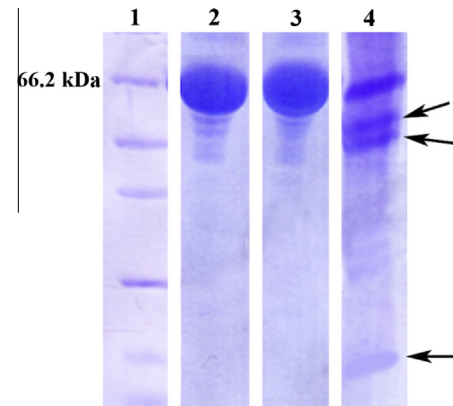
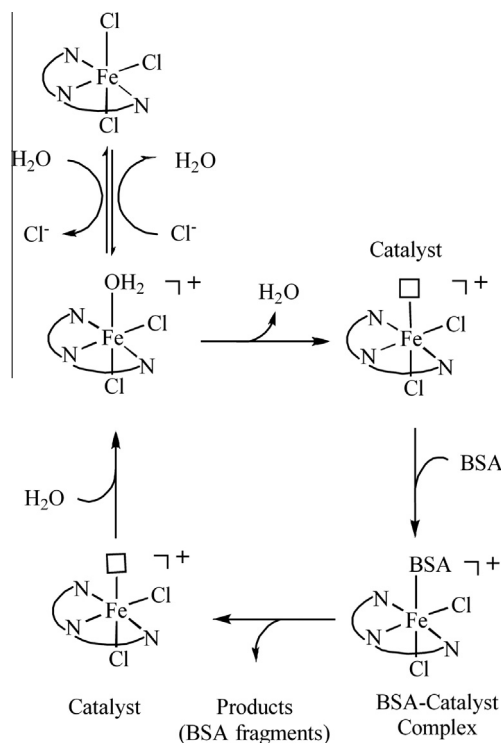


Fig. 14. SDS-PAGE of BSA, Lane 1: protein marker; Lane 2: BSA control solution I (4°C , in the dark); Lane 3: BSA control solution II (40°C , after 3 h in the dark); and Lane 4: BSA + complex (2) (0.05 mg , 40°C , after 3 h in the dark).

Furthermore, the differential pulse voltammograms for reduction of the complex indicate that the current decreases when CT-DNA is added (Fig. 10B). Also, a negative shift in E_p is observed for the complex. This change demonstrates an interaction between the complex and DNA, which is in consistent with the CV results.

DNA-binding study with viscosity measurements

Because of the sensitivity of DNA viscosity to DNA length change; its measurement upon addition of a compound is often concerned as the least ambiguous method to clarify the interaction mode of a compound with DNA and provides reliable evidence for the intercalative binding mode [64]. Viscosity measurement was carried out on CT DNA solution upon addition of increasing amount



Scheme 3. A proposed simple mechanism for the catalytic effect of (2) on the cleavage of BSA.

of complex (1) (Fig. 11). In the case of classic intercalation, DNA base pairs are segregated in order to host the bound compound resulting in the lengthening of the DNA helix and subsequently increased DNA viscosity. On the other hand, the binding of a compound exclusively in DNA grooves by means of partial and/or non-classic intercalation causes a bend or kink in the DNA helix

reducing its effective length and, as a result, DNA solution viscosity is decreased or remains unchanged [16c,18b,65]. Therefore, the observed increase of the relative viscosity of DNA upon addition of the complex can be explained by the insertion of the compounds between the DNA base pairs, leading to an increase in the separation of base pairs at intercalation sites and, thus, an increase in overall DNA length.

DNA cleavage studies

Investigation the DNA-cleavage ability of transition metal complexes is also useful as it can provide useful information about the toxicity mechanism and artificial nuclease. DNA-cleavage is controlled by relaxation of the supercoiled circular (SC) form of plasmid DNA into nicked circular (NC) and/or linear forms. In the DNA-cleavage reaction, three phenomena may be observed: (1) if circular plasmid DNA is run on horizontal gel electrophoresis, the fastest migration will be detected for the supercoiled form (Form I); (2) when one strand is cleaved, the supercoiled system will relax to produce a slower-moving open circular form (Form II); and (3) if both strands are cleaved, a linear form (Form III) will be generated, which migrates at an intermediate rate [65,66].

The $[\text{Fe}(\text{tpz})_2](\text{NO}_3)_2$ complex showed nuclease activity at concentrations of 5–100 μM . A concentration of 5 μM of the complex cleaves about 2% of the plasmid to yield the nicked circular form (Form II) (Fig. 12, Lane 2), whereas 100 μM of the complex causes more than 9% of the plasmid to give form II (Fig. 12, Lane 6). This phenomenon illustrates that the DNA cleavage activity of the complex is obviously dependent on the complex concentration.

In order to understand the mechanistic pathway involved in the DNA cleavage reaction, it was investigated by gel electrophoresis in the presence of various radical scavengers, such as NaN_3 , SOD and DMSO (Fig. 12, Lanes 7–9). The DNA-cleavage of the plasmid was inhibited significantly in the presence of NaN_3 suggesting that $^1\text{O}_2$ is likely to be the reactive species responsible for the nuclease activity (Fig. 12, Lane 7). The inhibitory activity of sodium azide can be attributed to the affinity of the azide anion for transition

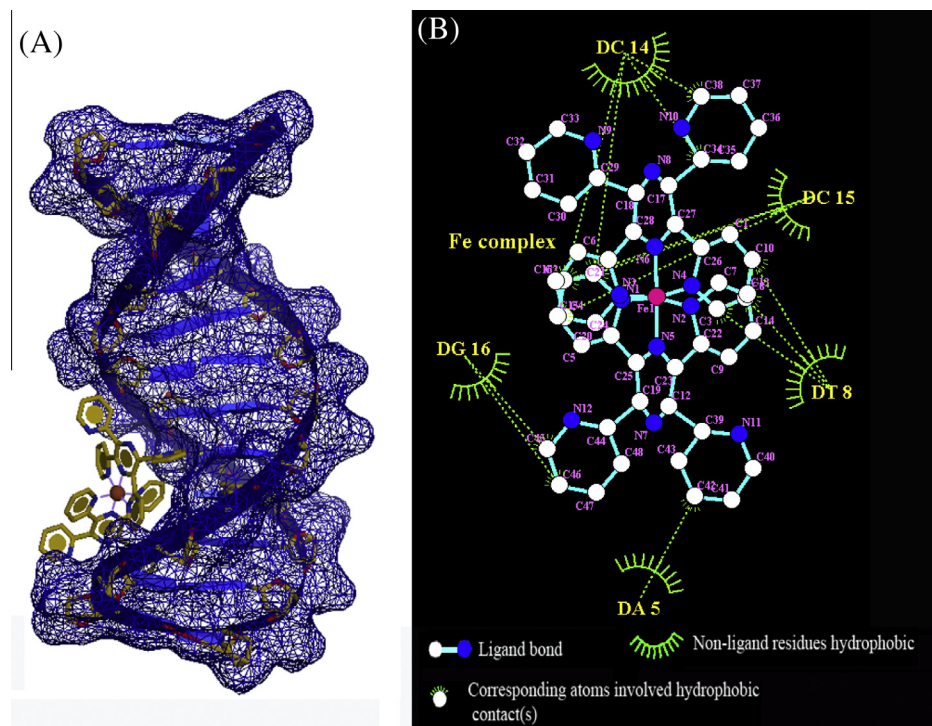


Fig. 15. (A) Presentation of the interaction of $[\text{Fe}(\text{tpz})_2](\text{NO}_3)_2$ with the major groove side of DNA by the UCSF Chimera, (B) the two-dimensional interactions are generated by LIGPLOT⁺.

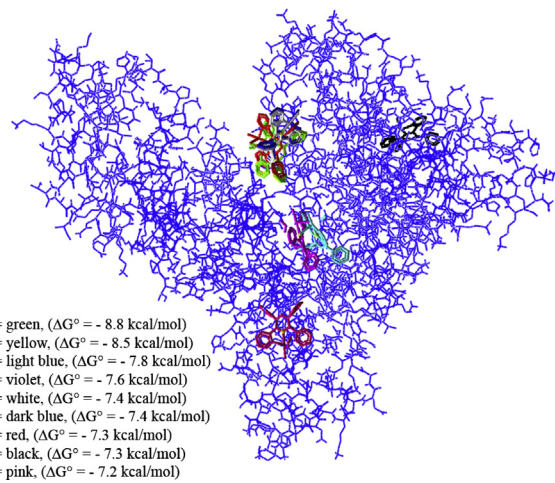


Fig. 16. The Fe(III) complex (2) docked in the binding pocket of BSA using MVD. The complex is depicted in a stick model, and BSA is represented in a wireframe model. The minimum free energy (ΔG°) of the docked structure is $-8.80 \text{ kcal mol}^{-1}$ (Poz 1, green). (For interpretation of the references to color in this figure legend, the reader is referred to the web version of this article.)

metals. SOD cannot inhibit the DNA cleavage. Combination of SOD with the Fe(II) complex accelerates the DNA cleavage and changes it to linear form, and consequently two lines are observed. Indeed, one line belongs to supercoiled and the other is for linear form of DNA (Fig. 12, Lane 8). When the hydroxyl radical scavenger DMSO was added to the reaction mixture, it was found to decrease the nuclease activity slightly which indicates a weak involvement of OH radicals in the cleavage process.

Also, the DNA cleavage activity of the complex in the presence of H_2O_2 was evaluated (Fig. 13). The cleavage activity of the complex was significantly enhanced by H_2O_2 . As shown in Fig. 13, the complex can convert the supercoiled plasmid DNA to the nicked DNA (Form II) in the presence of an activator. Control experiments with only H_2O_2 did not show any significant DNA cleavage under the similar experimental conditions (Fig. 13, Lane 2). In the presence of H_2O_2 , a concentration of $0.1 \mu\text{M}$ of the complex converted 18% of Form I to Form II (Fig. 13, Lane 3). With the increase of the complex concentration ($3 \mu\text{M}$), the percentage of Form II increased to 56% (Fig. 13, Lane 7). The cleavage ability of the complex increases when the concentration of the complex is increased (Fig. 13, Lanes 3–7). Therefore, it is concluded that the $[\text{Fe}(\text{tppz})_2](-\text{NO}_3)_2$ complex is a potential chemical nuclease.

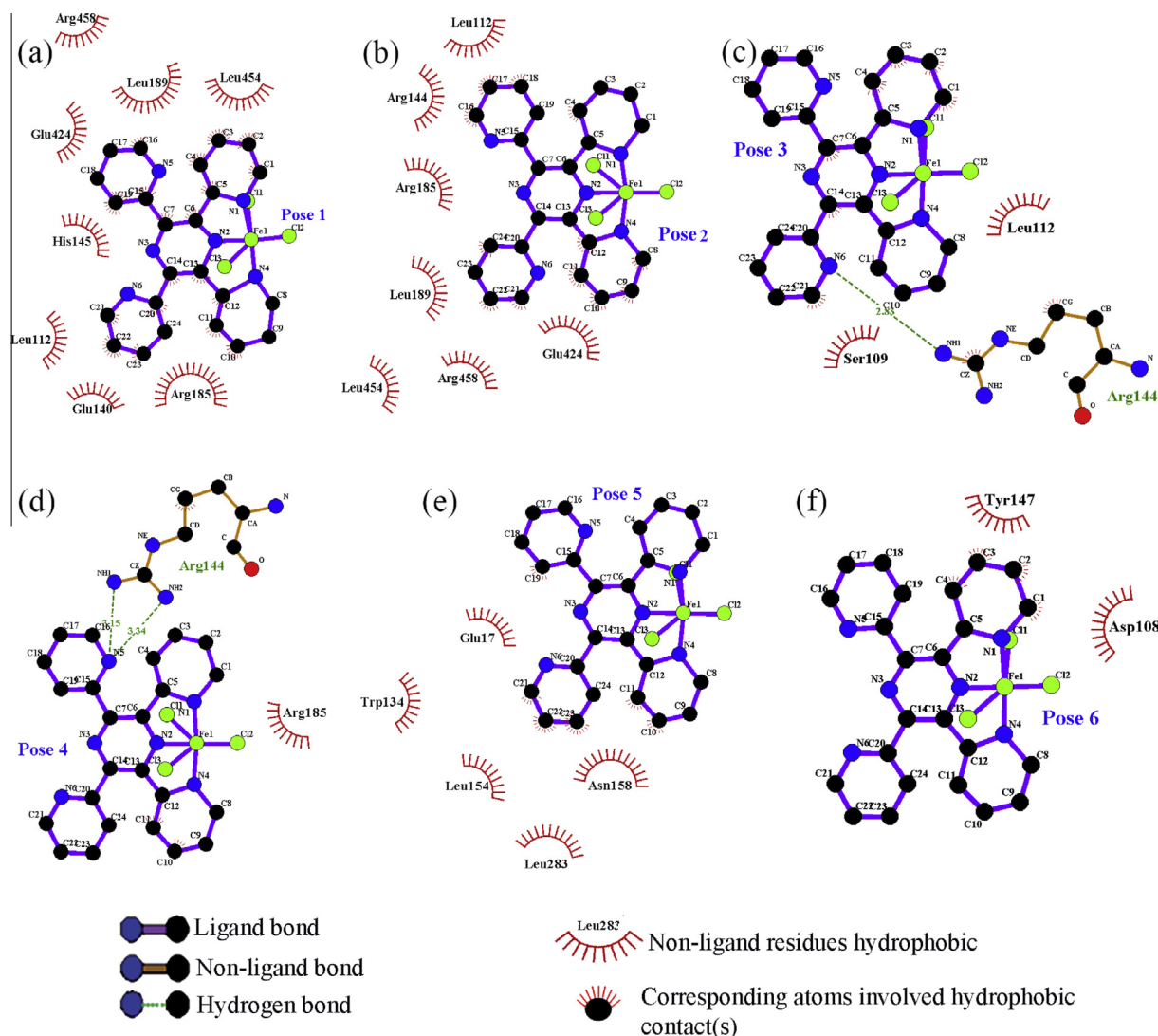


Fig. 17. Two-dimensional interactions of (2) with BSA generated by LIGPLOT⁺.

Catalytic effect of (2) on the BSA cleavage

Serum albumins as the major soluble protein constituents of the circulatory system have many physiological functions. They contribute to colloid osmotic blood pressure and are chiefly responsible for the maintenance of blood pH. The most remarkable property of albumins is that they serve as a depot and transport protein for numerous endogenous and exogenous compounds [67]. One of the serum albumins that most commonly used in research is bovine serum albumin (BSA). BSA has been used as a catalyst [68] and also its cleavage has been studied by different compounds [69]. The catalytic effects of some materials on proteins such as BSA have been also investigated [70] but according to our literature survey, there is no any report for the catalytic effect of polypyridyl metal complexes on the BSA cleavage. Therefore, the catalytic effect of the water-insoluble Fe(III) complex (2) on BSA has been studied.

The SDS-PAGE results of the catalytic effect on the BSA cleavage are shown in Fig. 14. BSA was cleaved significantly in the presence of (2), suggesting that the Fe(III) complex can catalyze the cleavage of BSA at 40 °C (Fig. 14, Lane 4). Two control solutions I and II (Lane 2 and Lane 3) have no any significant change in the absence of (2) at 4 and 40 °C in the dark. A simple catalytic cycle for the BSA cleavage is proposed in Scheme 3. In the first step, one Cl⁻ ligand of (2) is displaced by water at 40 °C. In the second step, dissociation of an aqua ligand from the [Fe(tppz)(H₂O)Cl₂]⁺ intermediate generates an empty coordination site on the Fe(III) ion in the presence of

BSA. In the third step, nucleophilic attack occurs on the Fe(III) center by BSA. In the fourth step, the coordinated BSA molecule cleaves into smaller fragments and leaves the inner coordination sphere of the Fe(III) ion. The Fe(III) cation is a Lewis acid and it might also be expected to catalyze the cleavage of BSA. The σ and the π polarization of the carbonyl groups (C=O) by Fe(III) have an important role in the bond-cleavage process in BSA [71].

Molecular docking

Molecular docking can be used to predict the affinity and binding orientation of a drug to its target (protein and DNA). In this study, the binding mode and intermolecular interactions of [Fe(tppz)₂](NO₃)₂ with DNA and (2) with BSA were investigated by molecular docking. The best conformer of target was taken from the MD simulation and used for docking. The coordination sphere of [Fe(tppz)₂](NO₃)₂ and (2) were generated from their X-ray crystal structures as a CIF file. The CIF files were converted to the PDB format using Mercury software [72].

Molecular docking of [Fe(tppz)₂](NO₃)₂ with DNA sequence d(ACCGACGTCGGT)₂

In order to obtain the binding site, blind docking was performed on a DNA duplex with sequence d(ACCGACGTCGGT)₂. In the blind docking of [Fe(tppz)₂](NO₃)₂ into DNA, the grid map set to 26 × 20 × 18 Å³ along the x, y, and z axes with 1.0 Å grid spacing. The center of grid map was set to -9.78, 52.664, and 0.149 Å.

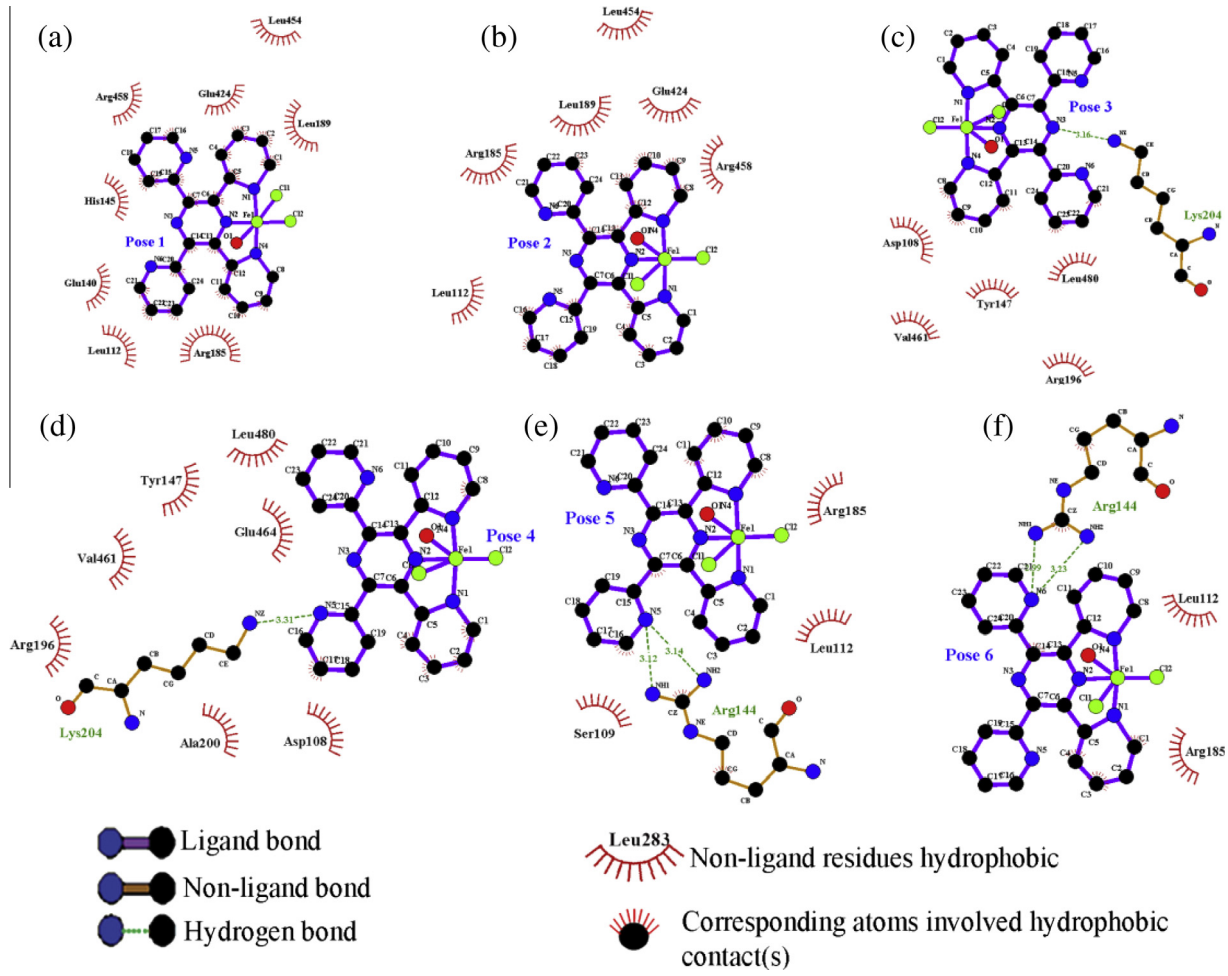


Fig. 18. Two-dimensional interactions of the aqua intermediate [Fe(tppz)(H₂O)Cl₂]⁺ with BSA generated by LIGPLOT+.

The conformations were ranked based on the lowest free binding energy. The results of docking model reveal that the complex fits into the DNA major groove. There are five categories of hydrophobic contacts between the complex atoms and bases of DNA, viz. (i) between C42 and DA5, (ii) between C3, C8, C10 and DT8, (iii) between C2, C11, C38, N10 and DC14, (iv) between C2, C11, C15 and DC15, and (v) between C45, C46 and DG16 (Fig. 15). The minimum binding free energy (ΔG°) of the docked structure of the complex with DNA is $-6.80 \text{ kcal mol}^{-1}$. The K_b value for the complex from the binding free energy (ΔG°) is found to be $6.2 \times 10^4 \text{ M}^{-1}$. This value indicates a high affinity of the complex for binding to DNA and is in good agreement with the experimental results.

That indicates a good binding affinity between the Fe(II) complex and DNA.

Molecular docking of (2) with BSA

In the docking of (2) into BSA, a grid map of dimensions $52 \times 40 \times 40 \text{ \AA}^3$ with a grid-point spacing of 1.0 \AA was created. The center of grid box was placed in points of 42.129, 69.009 and 69.245 \AA . The conformations were ranked based on the lowest free binding energy. The molecular docking study of BSA showed that the complex (2) prefers the binding pocket of domain II. The poses were ranked based on the lowest free binding energy (Fig. 16). To explain how the operation of a catalytic effect of (2) on the BSA cleavage, the molecular docking study was performed in two steps. In the first step, complex (2) was studied, and in the second step, the aqua intermediate $[\text{Fe}(\text{tppz})(\text{H}_2\text{O})\text{Cl}_2]^+$ (see Scheme 3) was investigated by molecular docking. As is clear in Fig. 17, (2) is suited docking within domain II. There are three hydrogen bonds between (2) and Arg144. The first hydrogen bond occurs between N6 and Arg144, length 2.83 \AA and the other two hydrogen bonds are between the N5 and Arg144, lengths 3.15 and 3.44 \AA , respectively (Fig. 17c and d). Also, there are several categories hydrophobic contacts between the complex (2) atoms and the amino acids of the binding site (Fig. 17). The minimum free energy (ΔG°) for the docked structure of (2) with BSA is $-8.80 \text{ kcal mol}^{-1}$, which indicates a high binding affinity between BSA and the complex.

The aqua intermediate $[\text{Fe}(\text{tppz})(\text{H}_2\text{O})\text{Cl}_2]^+$ shows more hydrogen bonds with BSA. As is clear in Fig. 18, there are four categories hydrogen bonds between $[\text{Fe}(\text{tppz})(\text{H}_2\text{O})\text{Cl}_2]^+$ and the amino acids, viz. (i) between N3 and Lys204, length 3.16 \AA (Fig. 18c), (ii) between N5 and Lys204, length 3.31 \AA (Fig. 18d), (iii) between N5 and Arg144, lengths 3.12 and 3.14 \AA (Fig. 18e), and (iv) between N6 and Arg144, lengths 2.99 and 3.23 \AA (Fig. 18f). These interactions show that, when the chloro ligand is replaced by water, the BSA molecule can easily approach the aqua intermediate $[\text{Fe}(\text{tppz})(\text{H}_2\text{O})\text{Cl}_2]^+$. Thus, the Fe(III) complex can effectively exert its catalytic role on BSA cleavage. In addition, there are several categories of hydrophobic contacts between $[\text{Fe}(\text{tppz})(\text{H}_2\text{O})\text{Cl}_2]^+$ and the amino acids of binding site (Fig. 18).

Conclusion

Two mononuclear iron complexes, containing tppz, $[\text{Fe}(\text{tppz})_2](\text{PF}_6)_2 \cdot \text{H}_2\text{O}$ and $\text{Fe}(\text{tppz})\text{Cl}_3 \cdot 2\text{CHCl}_3$, were prepared and structurally characterized by X-ray crystallography. The interaction of $[\text{Fe}(\text{tppz})_2](\text{NO}_3)_2$ with CT-DNA was monitored by spectroscopic and voltammetric measurements followed by molecular docking. The results indicate that the complex can interact with CT-DNA by three bidding modes: electrostatic, groove, and partial insertion. The capability of the polypyridyl Fe(II) complex to interact with DNA can be useful in designing and developing new coordination compounds as potential therapeutic agents. For the first time, we

indicated that the polypyridyl Fe(III) complex (2) can act as a catalyst for BSA cleavage at 40°C .

Acknowledgements

We are grateful to the Isfahan University of Technology (IUT) for financial support. We also thank the University of Otago for purchase of the diffractometer.

Appendix A. Supplementary material

Crystallographic data for $[\text{Fe}(\text{tppz})_2](\text{PF}_6)_2 \cdot \text{H}_2\text{O}$ and $\text{Fe}(\text{tppz})\text{Cl}_3 \cdot 2\text{CHCl}_3$ have been deposited with the Cambridge Crystallographic Data Centre, CCDC 978851 and CCDC 978852, respectively. Supplementary data associated with this article can be found, in the online version, at <http://dx.doi.org/10.1016/j.saa.2014.06.105>.

References

- [1] (a) M.N. Patel, D.S. Gandhi, P.A. Parmar, *Spectrochim. Acta, Part A* 84 (2011) 243–248;
(b) P.N. Patel, N. Singh, K.K. Shukla, V.L.N. Gundla, U.K. Chauhan, *Spectrochim. Acta, Part A* 63 (2006) 21–26.
- [2] (a) A. Velázquez-Palenzuela, L. Zhang, L. Wang, P.L. Cabot, E. Brillas, K. Tsay, J. Zhang, *Electrochim. Acta* 56 (2011) 4744–4752;
(b) X.B. Fu, Z.H. Lin, H.F. Liu, X.Y. Le, *Spectrochim. Acta, Part A* 122 (2014) 22–33.
- [3] (a) H. Hadadzadeh, M. Salimi, M. Weil, M.T. Behnamfar, F. Darabi, *Polyhedron* 53 (2013) 179–186;
(b) H. Hadadzadeh, Gh. Mansouri, A. Rezvani, H.R. Khavasi, B.W. Skelton, M. Makha, F. Rostami Charati, *Polyhedron* 30 (2011) 2535–2543.
- [4] H.A. Goodwin, F. Lions, *J. Am. Chem. Soc.* 81 (1959) 6415–6422.
- [5] (a) H. Hadadzadeh, A.R. Rezvani, G.P.A. Yap, R.J. Crutchley, *Inorg. Chim. Acta* 358 (2005) 1289–1292;
(b) E. Burkholder, V. Golub, C.J. ÓConnor, J. Zubietta, *Inorg. Chem.* 43 (2004) 7014–7029;
(c) L. Luo, L. Qiu, B. Liu, X. Zhang, F. Yang, L. Cui, *Chin. J. Chem.* 30 (2012) 522–528.
- [6] S. Saragnapani, U.S. Patent 447, 1997, p. 114.
- [7] A. Velázquez-Palenzuela, L. Zhang, L. Wang, P.L. Cabot, E. Brillas, K. Tsay, J. Zhang, *J. Phys. Chem. C* 115 (2011) 12929–12940.
- [8] S. Zhao, S.M. Arachchige, C. Slebodnick, K.J. Brewer, *Inorg. Chem.* 47 (2008) 6144–6152.
- [9] W.A. Alves, V. Pfaffen, P.I. Ortiz, S.I. Córdoba de Torresi, R.M. Torresi, *J. Braz. Chem. Soc.* 19 (2008) 651–659.
- [10] S.E. Herrick, G.J. Laurent, U.K. Patent Appl. GB 2 376, 2002, p. 886.
- [11] S. Fantacci, F. De Angelis, J. Wang, S. Bernhard, A. Selloni, *J. Am. Chem. Soc.* 126 (2004) 9715–9723.
- [12] (a) J.R. Lakowicz, F. Castellano, Z. Murtaza, *Int. Pat. Appl. WO* 9 (1999) 936–779;
(b) W.A. Alves, P.A. Fiorito, S.I. Córdoba de Torresi, R.M. Torresi, *Biosens. Bioelectron.* 22 (2006) 298–305;
- [13] (c) J. Yuasa, S. Fukuzumi, *J. Am. Chem. Soc.* 130 (2008) 566–575.
- [14] (d) S. Flores-Torres, G.R. Hutchison, L.J. Soltzberg, H.D. Abruña, *J. Am. Chem. Soc.* 128 (2006) 1513–1522.
- [15] K. Brewer, S. Swavey, U.S. Patent Appl. U.S. 2,003,280,767, 2003.
- [16] (a) F. Hajareh Haghighi, H. Hadadzadeh, F. Darabi, Z. Jannesari, M. Ebrahimi, T. Khayamian, M. Salimi, H. Amiri Rudbari, *Polyhedron* 65 (2013) 16–30;
(b) A.J. Prussin, S. Zhao, A. Jain, B.S.J. Winkel, K.J. Brewer, *J. Inorg. Biochem.* 103 (2009) 427–431;
(c) S. Rubino, P. Portanova, A. Girasolo, G. Galvaruso, S. Oreccchio, G.C. Stocco, *Eur. J. Med. Chem.* 44 (2009) 1041–1048.
- [17] (d) K. Abdi, H. Hadadzadeh, M. Salimi, J. Simpson, A. Dehno Khalaji, *Polyhedron* 44 (2012) 101–112;
- [18] (b) K. Abdi, H. Hadadzadeh, M. Weil, M. Salimi, *Polyhedron* 31 (2012) 638–648;
- [19] (c) N. Shahabadi, S. Kashanian, F. Darabi, *Eur. J. Med. Chem.* 45 (2010) 4239–4245.
- [20] B. Peng, H. Chao, B. Sun, F. Gao, L.N. Ji, J. Zhang, *Transition Met. Chem.* 32 (2007) 271–277.
- [21] (a) F. Dimiza, A.N. Papadopoulos, V. Tangoulis, V. Psycharis, C.P. Raptopoulou, D.P. Kissisoglu, G. Psomas, *Dalton Trans.* 39 (2010) 4517–4528;
- [22] (b) F. Dimiza, A.N. Papadopoulos, V. Tangoulis, V. Psycharis, C.P. Raptopoulou, D.P. Kissisoglu, G. Psomas, *J. Inorg. Biochem.* 107 (2012) 54–64.
- [23] (c) L.M. Chen, J. Liu, J.C. Chen, S. Shi, J. Mol. Struct. 881 (2008) 156–166.
- [24] S. Arturo, B. Giampaolo, R. Giuseppe, L.G. Maria, T. Salvatore, *J. Inorg. Biochem.* 98 (2004) 589–594.
- [25] W. Lewandowski, M. Kalinowska, H. Lewandowska, *J. Inorg. Biochem.* 99 (2005) 1407–1423.

- [22] R. Chen, C.S. Liu, H. Zhang, Y. Guo, X.H. Bu, M. Yang, *J. Inorg. Biochem.* 101 (2007) 412–421.
- [23] J. Marmur, *J. Mol. Biol.* 3 (1961) 208–218.
- [24] M.E. Reichmann, S.A. Rice, C.A. Thomas, P. Doty, *J. Am. Chem. Soc.* 76 (1954) 3047–3053.
- [25] G.M. Sheldrick, SADABS, A Program for Empirical Absorption and other Corrections, University of Göttingen, Germany, 1997.
- [26] G.M. Sheldrick, *Acta Crystallogr., Sect. A* 64 (2007) 112–122.
- [27] O. Trott, A.J. Olson, *J. Comput. Chem.* 31 (2010) 455–461.
- [28] E.F. Petterson, T.D. Goddard, C.C. Huang, G.S. Couch, *J. Comput. Chem.* 25 (2004) 1605–1612.
- [29] R.A. Laskowski, M.B. Swindells, *J. Chem. Inf. Model.* 51 (2011) 2778–2786.
- [30] D.V. Spoel, E. Lindahl, B. Hess, G. Groenhof, A.E. Mark, H.J.C. Berendsen, *J. Comput. Chem.* 26 (2005) 1701–1718.
- [31] V. Hornak, R. Abel, A. Okur, B. Strockbine, A. Roitberg, C. Simmerling, *Struct. Funct. Bioinform.* 65 (2006) 712–725.
- [32] T. Darden, D. York, L. Pedersen, *J. Chem. Phys.* 98 (1993) 10089–10092.
- [33] U. Essmann, L. Perera, M.L. Berkowitz, T. Darden, H. Lee, L.G. Pedersen, *J. Chem. Phys.* 103 (1995) 8577–8593.
- [34] W.C. Swope, H.C. Andersen, P.H. Berens, K.R. Wilson, *J. Chem. Phys.* 76 (1982) 637–649.
- [35] K. Huang, *Statistical Mechanics*, Wiley, New York, 1963.
- [36] L. Rivail, C. Chipot, B. Maigret, I. Bestel, S. Sicsic, M. Tarek, *Theochem. J. Mol. Struct.* 817 (2007) 19–26.
- [37] H.J.C. Berendsen, J.P.M. Postma, W.F.V. Gunsteren, A.D. Nola, J.R. Haak, *J. Chem. Phys.* 81 (1984) 3684–3690.
- [38] M. Maekawa, T. Minematsu, H. Konaka, K. Sugimoto, T. Kuroda-Sowa, Y. Suenaga, M. Munakata, *Inorg. Chim. Acta* 357 (2004) 3456–3472.
- [39] C.W. Padgett, W.T. Pennington, T.W. Hanks, *Cryst. Growth Des.* 5 (2005) 737–744.
- [40] C.W. Padgett, R.D. Walsh, G.W. Drake, T.W. Hanks, W.T. Pennington, *Cryst. Growth Des.* 5 (2005) 745–753.
- [41] L.M. Toma, D. Armentano, G. De Munno, J. Sletten, F. Lloret, M. Julve, *Polyhedron* 26 (2007) 5263–5270.
- [42] A.B.P. Lever, *Inorganic Electronic Spectroscopy*, Elsevier, Amsterdam, 1984.
- [43] K. Nakamoto, *Infrared and Raman Spectra of Inorganic and Coordination Compounds*, in: Part II: Application in Coordination, Organometallic and Bioinorganic Chemistry, fifth ed., Wiley-Interscience, New York, 2009.
- [44] M. Daryanvard, H. Hadadzadeh, A. Dehno Khalaji, M. Weil, *Transition Met. Chem.* 34 (2009) 779–786.
- [45] P.J. Cox, G. Psomas, C.A. Bolos, *Bioorg. Med. Chem.* 17 (2009) 6054–6062.
- [46] F. Arjmand, M. Muddassir, *J. Photochem. Photobiol. B* 101 (2010) 37–46.
- [47] F.J. Chen, M. Xu, P.X. Xi, H.Y. Liu, Z.Z. Zeng, *Spectrochim. Acta A* 81 (2011) 21–27.
- [48] A. Wolfe, G.H. Shimer, T. Meehan, *Biochemistry* 26 (1987) 6392–6396.
- [49] A. Jayamani, V. Thamilarasan, N. Sengottuvelan, P. Manisankar, S.K. Kang, Y.I. Kim, V. Ganeshan, *Spectrochim. Acta, Part A* 122 (2014) 365–374.
- [50] J.R. Lakowicz, G. Weber, *Biochemistry* 12 (1973) 4161–4170.
- [51] S. Tabassum, W.M. Al-Asbahy, M. Afzal, M. Shamsi, F. Arjmand, *J. Lumin.* 132 (2012) 3058–3065.
- [52] Y. Lu, M. Xu, G. Wang, Y. Zheng, *J. Lumin.* 131 (2011) 926–930.
- [53] D.S. Raja, N.S.P. Bhuvanesh, K. Natarajan, *Inorg. Chim. Acta* 385 (2012) 81–93.
- [54] V.I. Ivanov, L.E. Minchenkova, A.K. Schyolkina, A.I. Poletayer, *Biopolymers* 12 (1973) 89–110.
- [55] S. Bi, H. Zhang, C. Qiao, Y. Sun, C. Liu, *Spectrochim. Acta A* 69 (2008) 123–129.
- [56] S. Bi, C. Qiao, D. Song, Y. Tian, D. Gao, Y. Sun, H. Zhang, *Sens. Actuators B: Chem.* 119 (2006) 199–208.
- [57] N. Shahabadi, M. Falsafi, *Spectrochim. Acta, Part A* 125 (2014) 154–159.
- [58] R. Indumathy, T. Weyhermuller, B. Unni Nair, *Dalton Trans.* 39 (2010) 2087–2097.
- [59] G. Zhang, X. Hu, P. Fu, *J. Photochem. Photobiol. B* 108 (2012) 53–61.
- [60] F. Arjmand, G. Chandra Sharma, M. Muddassir, S. Tabassum, *Chirality* 23 (2011) 557–567.
- [61] P. Zanello, *Inorganic Electrochemistry, Theory, Practice and Application*, RSC, Cambridge, UK, 2003.
- [62] M.T. Carter, M. Rodriguez, A.J. Bard, *J. Am. Chem. Soc.* 111 (1989) 8901–8911.
- [63] K. Jiao, Q.X. Wang, W. Sun, F.F. Jian, *J. Inorg. Biochem.* 99 (2005) 1369–1375.
- [64] J.L. Garcia-Gimenez, M. Gonzalez-Alvarez, M. Liu-Gonzalez, B. Macias, J. Borras, G. Alzuet, *J. Inorg. Biochem.* 103 (2009) 923–934.
- [65] N. Shahabadi, F. Darabi, M. Maghsudi, S. Kashanian, *DNA Cell Biol.* 29 (2009) 329–336.
- [66] (a) H. Hadadzadeh, M. Salimi, M. Weil, M.T. Behnamfar, F. Darabi, *Polyhedron* 53 (2013) 179–186;
 (b) Q. Li, T.A. van den Berg, B.L. Feringa, G. Roelfes, *Dalton Trans.* 39 (2010) 8012–8021.
- [67] D.C. Carter, J.X. Ho, *Adv. Protein Chem.* 45 (1994) 153–203.
- [68] (a) R.P. Taylor, J.B. Vatz, *J. Am. Chem. Soc.* 95 (1973) 5819–5820;
 (b) B.A. Smith, H.R. Guttmann, J.R. Springfield, *Biochem. Pharmacol.* 15 (1989) 3987–3994;
 (c) R.C. Kolanczyk, I.R. Rutks, H.R. Guttmann, *Chem. Res. Toxicol.* 4 (1991) 187–194.
- [69] J. Chen, R. Wan, H. Liu, C.M. Chen, Y.F. Zhao, *Lett. Pept. Sci.* 7 (2000) 325–329.
- [70] I.S. Hong, U.S. Patent 9, 31, 2002.
- [71] R.G. Wilkins, *Kinetics and Mechanism of Reactions of Transition Metal Complexes*, 2nd thoroughly, Revised ed., Wiley-VCH, New York, 2002.
- [72] C.F. Macrae, I.J. Bruno, J.A. Chisholm, P.R. Edgington, P. McCabe, E. Pidcock, L. Rodriguez-Monge, R. Taylor, J. van de Streek, P.A. Wood, *J. Appl. Cryst.* 41 (2008) 466–470.